Electronic Supplementary Material (ESI) for Chemical Communications.

Supporting information for:

Cooperative Bond Activations by a Tucked-in Iron Complex

Joseph A. Zurakowski and Marcus W. Drover*

*E-mail: marcus.drover@uwindsor.ca

[a] Department of Chemistry and Biochemistry, The University of Windsor, 401 Sunset Avenue, Windsor, ON, N9B 3P4, Canada

Experimental Section:

General considerations. All experiments were carried out employing standard Schlenk techniques under an atmosphere of dry nitrogen employing degassed, dried solvents in a solvent purification system supplied by PPT, LLC. Non-halogenated solvents were tested with a standard purple solution of sodium benzophenone ketyl in tetrahydrofuran in order to confirm effective moisture removal. d_6-benzene was dried over molecular sieves and degassed by three freeze-pump-thaw cycles. All other reagents were purchased from commercial vendors and used without further purification unless otherwise stated. 1,2-*bis*(di-*n*-propylphosphino)ethane) (d*n*ppe),[1] $HBCy_2$,[2] and [Cp*Fe(d*n*ppe)Cl][3] were prepared according to literature procedures.

Physical methods. ^1H NMR spectra are reported in parts per million (ppm) and are referenced to residual solvent e.g., $^1H(C_6D_6)$: $\delta = 7.16$; $^{13}C(C_6D_6)$: $\delta = 128.06$; coupling constants are reported in Hz. ^{13}C, ^{31}P, and ^{11}B NMR spectra were performed as proton-decoupled experiments (unless explicitly stated otherwise) and are reported in ppm.

Preparation of Compounds:

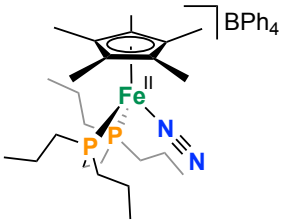

[Cp*Fe^{II}(d*n*ppe)N$_2$]BPh$_4$ (**1**; $C_{48}H_{67}BFeN_2P_2$, M_W = 801 g/mol): In the glovebox, [Cp*Fe(d*n*ppe)Cl] (500 mg, 1.02 mmol) was weighed into a 20 mL scintillation vial equipped with a stir bar. Approximately 10 mL of Et_2O was added. To this solution was added $NaBPh_4$ (107 mg, 0.31 mmol, 1 equiv.) suspended in 3 mL of Et_2O. The mixture was stirred for 1 h during which time it became yellow. The solvent was removed *in-vacuo* and the powder extracted into THF and filtered through Celite®. The orange filtrate was dried *in-vacuo* and the resulting orange powder was washed with 3 x 5 mL of pentane and dried (598 mg, 73%). Crystals suitable for X-Ray diffraction were grown from THF layered with pentane at -35 °C overnight. **^{1}H NMR (500 MHz, d$_8$-THF, 298 K):** δ_H = 7.26 (m; 8H; *o*-C$_6$H$_5$ [BPh$_4$]), 6.83 (m; 8H; *m*-C$_6$H$_5$ [BPh$_4$]), 6.69 (m, 4H; *p*-C$_6$H$_5$ [BPh$_4$]), 1.93 (m; 2H; P-CH$_2$-CH$_2$-P linker), 1.79 (m; 4H; overlapping P-CH$_2$-CH$_2$-CH$_3$ signals), 1.63 (m; 2H; overlapping P-CH$_2$-CH$_2$-CH$_3$ signals), 1.59 (s, 15H; Cp*-CH$_3$), 1.51-1.41 (m, 10H; overlapping P-CH$_2$-CH$_2$-CH$_3$ signals), 1.28 (m, 2H; P-CH$_2$-CH$_2$-P linker), 1.05-0.98 (overlapping triplets, 12H; P-CH$_2$-CH$_2$-CH$_3$). **^{13}C{^{1}H} NMR (125.8 MHz, d$_8$-THF, 298 K):** δ_C = 165.0 (q; [BPh$_4$]), 137.0 (s; *o*-C$_6$H$_5$ [BPh$_4$]), 125.5 (s; *m*-C$_6$H$_5$ [BPh$_4$]), 121.7 (s; *p*-C$_6$H$_5$ [BPh$_4$]), 91.9 (s; Cp*(aromatic)), 29.0-28.7 (m; overlapping CH$_2$ signals), 22.8 (m; CH$_2$), 18.7 (app. s; CH$_2$), 17.8 (m; CH$_2$), 16.2-15.9 (m; overlapping CH$_3$ signals), 9.97 (s; Cp*-CH$_3$). **^{31}P{^{1}H} NMR (202.5 MHz, d$_8$-THF, 298 K):** δ_P = +71.2. **^{11}B{^{1}H} NMR (160.5 MHz, d$_8$-THF, 298 K):** δ_B = -6.5 (s; BPh$_4$). **FT-IR (ATR):** 2098 cm^{-1} (ν[N$_2$]).

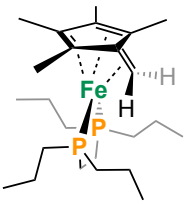

[(η^6-C$_5$Me$_4$=CH$_2$)Fe(d*n*ppe)] (**2**; $C_{24}H_{46}FeP_2$, M_W = 452 g/mol): In the glovebox, **1** (400 mg, 0.50 mmol) was weighed into a 20 mL scintillation vial equipped with a stir bar and dissolved in approximately 4 mL of THF. This solution was cooled to -35 °C in the glovebox freezer. Next, *n*-butyllithium (1.6 M in hexane, 1 equiv.) was added. The reaction was stirred for 30 min at room temperature. The solution became gradually red over time. The solvent was removed *in-vacuo*, and the product was extracted with 3 x 2 mL portions of pentane and filtered through Celite®. The red filtrate was dried *in vacuo* giving **2** as a red powder (192 mg, 85%). Crystals suitable for X-ray diffraction were grown from

a saturated pentane solution at -35 °C overnight. **^{1}H NMR (500 MHz, C_6D_6, 298 K):** δ_H = 2.74 (t; 2H; η^6-C_5Me_4=C$\underline{H}_2$ ($^3J_{H\text{-}P}$ = 3.6 Hz)), 1.70 (s; 12H; η^6-$C_5\underline{Me}_4$=CH_2), 1.63 (m; 2H; C$\underline{H}_2$), 1.51-1.45 (m; 8H; multiple overlapping C$\underline{H}_2$ signals), 1.37 (m; 3H; multiple overlapping C$\underline{H}_2$ signals), 1.20 (m; 7H; multiple overlapping C$\underline{H}_2$ signals), 0.96 (t; 6H; P-CH_2-CH_2-C$\underline{H}_3$ ($^3J_{H\text{-}H}$ = 7.24 Hz)), 0.92 (t; 6H; P-CH_2-CH_2-C$\underline{H}_3$ ($^3J_{H\text{-}H}$ = 7.24 Hz)). **^{13}C{^{1}H} NMR (75.5 MHz, C_6D_6, 298 K):** δ_C = 96.2 (s; η^6-[C_4Me_4]C$\underline{}$=CH_2), 84.0 (br. s; η^6-[$\underline{C}_4Me_4$]C=CH_2), 35.6 (m; $\underline{C}H_2$), 23.5 (m; η^5-[C_4Me_4]C=$\underline{C}H_2$), 28.3 (m; multiple overlapping $\underline{C}H_2$ signals), 19.0 (s; $\underline{C}H_2$), 18.3 (s; $\underline{C}H_2$), 16.7 (m; multiple overlapping P-CH_2-CH_2-$\underline{C}H_3$ signals), 12.7 (s; η^6-[$C_4\underline{Me}_4$]C=CH_2), 11.9 (s; η^6-[$C_4\underline{Me}_4$]C=CH_2). **^{31}P{^{1}H} NMR (202.5 MHz, C_6D_6, 298 K):** δ_P = +89.6.

[(η^5-C_5Me_4–CH_2–CO_2)Fe^{II}(d*n*ppe)] (**3**; $C_{25}H_{46}FeO_2P_2$, M_W = 496 g/mol): In the glovebox, **2** (20 mg, 0.04 mmol) was weighed into a J-Young NMR tube and dissolved in approximately 500 µL of THF. The J-Young NMR tube was removed from the glovebox and degassed with 3 freeze-pump-thaw cycles on the Schlenk line. After the third cycle, the J-Young NMR tube was warmed to room temperature and an atmosphere of CO_2 was introduced. The J-Young NMR tube was shaken vigorously for 5 mins then left to sit for 1 h. During this time, the solution changed from red to purple. The solvent was removed *in-vacuo* on the Schlenk line, then the tube brought back into the glovebox. The purple solid was extracted into THF and filtered through Celite®. The filtrate was dried *in-vacuo* and the purple solid washed with 3 x 2 mL of pentane, giving **3** (16 mg, 72%). Crystals suitable for X-ray diffraction were grown from slow evaporation of THF at room temperature overnight. **^{1}H NMR (500 MHz, C_6D_6, 298 K):** δ_H = 3.26 (br. s; 2H; η^5-C_5Me_4–C$\underline{H}_2$–CO_2), 2.07 (br. s; 6H; η^5-$C_5\underline{Me}_4$–CH_2–CO_2), 1.90 (m; 2H; C$\underline{H}_2$), 1.69 (m; 4H; multiple overlapping C$\underline{H}_2$ signals), 1.47 (m; 8H; multiple overlapping C$\underline{H}_2$ signals), 1.26 (m; 2H; C$\underline{H}_2$), 1.18 (m; 2H; C$\underline{H}_2$), 1.11 (m; 2H; C$\underline{H}_2$), 1.00 (br. t; 6H; P-CH_2-CH_2-C$\underline{H}_3$), 0.90 (br. s; 6H; η^5-$C_5\underline{Me}_4$–CH_2–CO_2), 0.86 (br. t; 6H; P-CH_2-CH_2-C$\underline{H}_3$). **^{13}C{^{1}H} NMR (125.8 MHz, C_6D_6, 298 K):** δ_C = 184.7 (app. s; η^5-C_5Me_4–CH_2–$\underline{C}O_2$ (assigned from a ^{1}H-^{13}C HMBC experiment), see Figure S14), 91.7 (s; η^5-$\underline{C}_5Me_4$–CH_2–CO_2), 82.2 (s; η^5-$\underline{C}_5Me_4$–CH_2–CO_2), 80.0 (s; η^5-$\underline{C}_5Me_4$–CH_2–CO_2), 32.9 (s; η^5-C_5Me_4–$\underline{C}H_2$–CO_2), 29.9 (m; $\underline{C}H_2$), 27.5 (m; $\underline{C}H_2$), 24.2 (m; $\underline{C}H_2$), 18.5 (m; $\underline{C}H_2$), 18.3 (m; CH_2), 16.6 (s; P-CH_2-CH_2-$\underline{C}H_3$), 16.4 (s; P-CH_2-

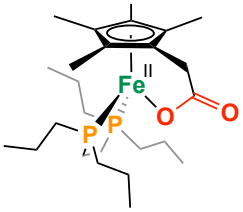

CH_2-$\underline{C}H_3$), 11.5 (s; η^5-$C_5\underline{Me}_4$–CH_2–CO_2), 11.3 (s; η^5-$C_5\underline{Me}_4$–CH_2–CO_2). **$^{31}P\{^1H\}$ NMR (121.5 MHz, C_6D_6, 298 K):** δ_P = +79.1. **IR (ATR):** 1622 cm^{-1} (ν[C=O]).

[±(η^5-C_5Me_4–CH_2–PhCHO)Fe^{II}(d*n*ppe)] **((±)-4**; $C_{31}H_{52}FeOP_2$, M_W = 559 g/mol): In the glovebox, **2** (20 mg, 0.04 mmol) was weighed into a 20 mL scintillation vial equipped with a stir bar and dissolved in approximately 4 mL of $PhCH_3$. Benzaldehyde (0.04 mmol, 4 µL, 1 equiv.) was added and the solution stirred overnight at room temperature. The solution became purple over time. The solvent was removed *in-vacuo* and the product extracted into 3 x 2 mL of pentane and filtered through Celite®. The solvent was removed *in-vacuo* giving **4** as a purple solid (18 mg, 82%). Crystals were grown by slow evaporation of pentane at room temperature. Connectivity map shown in Figure S36. **^1H NMR (300 MHz, C_6D_6, 298 K):** δ_H = 7.55 (m; 2H, Ph), 7.29 (m; 2H, Ph), 7.10 (m; 1H, Ph), 5.42 (m; 1H, η^5-C_5Me_4–CH_2–PhC$\underline{H}$O), 2.55 (app. d; 3H; η^5-$C_5\underline{Me}_4$–CH_2–PhCHO), 2.46-2.36 (m; 2H; η^5-C_5Me_4–$C\underline{H}_2$–PhCHO), 2.30 (app. d; 3H; η^5-$C_5\underline{Me}_4$–CH_2–PhCHO), 2.08-2.03 (3H; multiple overlapping $C\underline{H}_2$ signals), 1.92-1.86 (2H, multiple overlapping $C\underline{H}_2$ signals), 1.60-1.48 (4H; multiple overlapping $C\underline{H}_2$ signals), 1.48-1.18 (11H; multiple overlapping $C\underline{H}_2$ signals), 1.13 (s; 3H; η^5-$C_5\underline{Me}_4$–CH_2-PhCHO), 1.10 (s; 3H; η^5-$C_5\underline{Me}_4$–CH_2-PhCHO), 0.98-0.85 (12H; multiple overlapping P-CH_2-CH_2-$C\underline{H}_3$ signals). **$^{13}C\{^1H\}$ NMR (75.5 MHz, C_6D_6, 298 K):** δ_C = 152.5 (s; quaternary $\underline{C}$ (Ph)), 127.0 (s; Ph), 125.9 (s; Ph), 125.5 (s; Ph), 109.2 (s; η^5-$\underline{C}_5Me_4$–CH_2-PhCHO), 93.8 (m; η^5-C_5Me_4–CH_2-Ph$\underline{C}$HO), 83.8-79.2 (overlapping Cp*-(aromatic) signals), 38.0 (s; η^5-C_5Me_4–$\underline{C}H_2$-PhCHO), 30.9-30.2 (multiple overlapping $\underline{C}H_2$ signals), 25.8-23.6 (multiple overlapping $\underline{C}H_2$ signals), 19.1-18.3 (multiple overlapping $\underline{C}H_2$ signals), 17.0-16.5 (multiple overlapping $\underline{C}H_3$ signals), 13.7 (s; $\underline{C}H_3$), 12.9 (s; $\underline{C}H_3$), 12.3 (s; $\underline{C}H_3$), 11.9 (s; $\underline{C}H_3$), 11.5 (s; $\underline{C}H_3$). **$^{31}P\{^1H\}$ NMR (121.5 MHz, C_6D_6, 298 K):** δ_P = +80.5 (d; $^2J_{P\text{-}P}$ = 33.7 Hz), +78.2 (d; $^2J_{P\text{-}P}$ = 33.7 Hz).

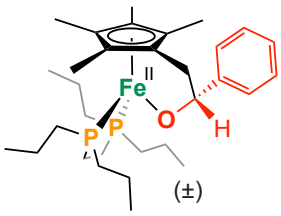

[(η⁵-C_5Me_4–CH_2–Au-(PPh_3))Fe^{II}(d*n*ppe)Br] (**5**; $C_{42}H_{61}AuBrFeP_3$, M_W = 992 g/mol): In the glovebox, **2** (20 mg, 0.04 mmol) was weighed into a 20 mL scintillation vial equipped with a stir bar and dissolved in approximately 4 mL of $PhCH_3$. Bromo(triphenylphosphine)gold(I) (0.04 mmol, 22 mg, 1 equiv.) was added and the solution stirred for 1 h at room temperature. The solution became gradually darker over time. The solvent was removed *in-vacuo* and the product extracted into 3 x 2 mL of pentane and filtered through Celite®. The solvent was removed *in-vacuo* giving **5** (15 mg, 34%). **^{1}H NMR (300 MHz, d_8-toluene, 298 K):** δ_H = 7.30 (br. m; 6H; Ph [PPh_3]), 7.11 (br. s; 3H; Ph [PPh_3]), 7.03-6.99 (Ph signal coincident with residual toluene (from d_8-toluene) signals), 2.55 (br. s; 2H; η⁵-C_5Me_4–C<u>H</u>$_2$–Au-PPh_3), 2.31 (br. m; 6H; multiple overlapping C<u>H</u>$_2$ signals), 1.99 (s; 6H; η⁵-C_5<u>Me</u>$_4$–CH_2–Au-(PPh_3)), 1.96 (s; 6H; η⁵-C_5<u>Me</u>$_4$–CH_2–Au-(PPh_3)), 1.89 (br. s; 2H; C<u>H</u>$_2$), 1.77 (br. s; 2H; C<u>H</u>$_2$), 1.70 (br. s; 2H; C<u>H</u>$_2$), 1.59 (br. m; 2H; C<u>H</u>$_2$), 1.48 (br. m; 4H; multiple overlapping C<u>H</u>$_2$ signals), 1.36 (br. s; 2H; C<u>H</u>$_2$), 1.11 (br. t; 6H; P-CH_2-CH_2-C<u>H</u>$_3$), 0.99 (br. t; 6H; P-CH_2-CH_2-C<u>H</u>$_3$). **^{13}C{^{1}H} NMR (125.8 MHz, d_8-toluene, 298 K):** δ_C = 134.4 (d; Ph-(aromatic)), 130.6 (m; Ph-(aromatic)), 100.9 (s; η⁵-<u>C</u>$_5$Me$_4$–CH_2–Au-(PPh_3)), 84.9 (s; η⁵-<u>C</u>$_5$Me$_4$–CH_2–Au-(PPh_3)), 73.6 (s; η⁵-<u>C</u>$_5$Me$_4$–CH_2–Au-(PPh_3)), 32.2 (m; <u>C</u>H$_2$), 31.3 (m; <u>C</u>H$_2$), 30.3 (m; <u>C</u>H$_2$), 28.3 (br. m; η⁵-C_5Me_4–<u>C</u>H$_2$–Au-PPh_3; assigned from a ^{1}H-^{13}C HSQC experiment), 24.2-24.0 (mulitple overlapping <u>C</u>H$_2$ signals), 19.7 (m; <u>C</u>H$_2$), 18.7 (m; <u>C</u>H$_2$), 16.9-16.8 (multiple overlapping P-CH_2-CH_2-<u>C</u>H$_3$ signals), 12.4 (s; η⁵-C_5<u>Me</u>$_4$–CH_2–Au-PPh_3), 12.2 (s; η⁵-C_5<u>Me</u>$_4$–CH_2–Au-PPh_3). *Note:* Other Ph-(aromatic) peaks (for PPh_3) coincident with d_8-toluene solvent peaks in ^{13}C{^{1}H} NMR spectrum. **^{31}P{^{1}H} NMR (202.5 MHz, d_8-toluene, 298 K):** δ_P = +77.9 (s; d*n*ppe), +40.3 (br; PPh_3).

[{η⁵-C_5Me_4–CH_2–$B(C_6F_5)_3$}Fe^{II}(d*n*ppe)N_2] (**6**; $C_{42}H_{46}BF_{15}FeN_2P_2$, M_W = 992 g/mol): In the glovebox, **2** (20 mg, 0.04 mmol) was weighed into a 20 mL scintillation vial equipped with a stir bar and dissolved in approximately 4 mL of THF. Tris(pentafluorophenyl)borane (0.04 mmol, 21 mg, 1 equiv.) was added and the solution stirred for 1 h at room temperature. The solution became yellow over time. The solvent was removed *in-vacuo* and

the product washed with 3 x 2 mL of pentane. The product was dried *in-vacuo* giving the titled compound as a yellow solid (31 mg, 70%). Crystals suitable for X-ray diffraction were grown by slow evaporation of THF at room temperature overnight. **^{1}H NMR (300 MHz, d$_8$-THF, 298 K):** δ_H = 2.55 (br. s; 2H; η^5-C$_5$Me$_4$–C<u>H</u>$_2$–B(C$_6$F$_5$)$_3$), 2.19-2.14 (m; 2H, multiple overlapping C<u>H</u>$_2$ signals), 1.95-1.88 (m; 6H, multiple overlapping C<u>H</u>$_2$ signals), 1.66 (s; 6H; η^5-C$_5$<u>Me</u>$_4$–CH$_2$–B(C$_6$F$_5$)$_3$), 1.59-1.55 (m; 12H, multiple overlapping C<u>H</u>$_2$ signals), 1.12-1.07 (m; 12H, multiple overlapping P-CH$_2$-CH$_2$-C<u>H</u>$_3$ signals), 0.99 (s; 6H, η^5-C$_5$<u>Me</u>$_4$–CH$_2$–B(C$_6$F$_5$)$_3$). **^{13}C{^{1}H} NMR (125.8 MHz, d$_8$-THF, 298 K):** δ_C = 149.1 (m; <u>C</u>-F(aromatic) [B(C$_6$F$_5$)$_3$]), 138.1 (m; <u>C</u>-F(aromatic) [B(C$_6$F$_5$)$_3$]), 127.0 (br; <u>C</u>-F(aromatic) [B(C$_6$F$_5$)$_3$]), 112.6 (app. s; quaternary <u>C</u>-(aromatic) [B(C$_6$F$_5$)$_3$]), 93.3 (s; η^5-<u>C</u>$_5$Me$_4$–CH$_2$–B(C$_6$F$_5$)$_3$), 92.0 (s; η^5-<u>C</u>$_5$Me$_4$–CH$_2$–B(C$_6$F$_5$)$_3$), 86.5 (s; η^5-<u>C</u>$_5$Me$_4$–CH$_2$–B(C$_6$F$_5$)$_3$), 30.4 (app. s; <u>C</u>H$_2$), 29.6-28.5 (multiple overlapping <u>C</u>H$_2$ signals), 22.9-22.6 (overlapping η^5-C$_5$Me$_4$–<u>C</u>H$_2$–B(C$_6$F$_5$)$_3$ and <u>C</u>H$_2$ signals), 18.9 (br. s; <u>C</u>H$_2$), 17.7 (br. s; <u>C</u>H$_2$), 16.1 (br. s; P-CH$_2$-CH$_2$-<u>C</u>H$_3$), 15.9 (br. s; P-CH$_2$-CH$_2$-<u>C</u>H$_3$), 9.9 (overlapping η^5-C$_5$<u>Me</u>$_4$–CH$_2$–B(C$_6$F$_5$)$_3$ signals). **^{31}P{^{1}H} NMR (202.5 MHz, d$_8$-THF, 298 K):** δ_P = +73.4. **^{19}F{^{1}H} NMR (282.4 MHz, d$_8$-THF, 298 K):** δ_F = -127.1 (br. s), -161.5 (m), -164.7 (br. s). **^{11}B{^{1}H} NMR (96.3 MHz, d$_8$-THF, 298 K):** δ_B = -14.7. **FT-IR (ATR):** 2093 cm^{-1} (ν[N$_2$]).

[{η^5-C$_5$Me$_4$–CH$_2$–B(Cy$_2$)}Fe^{II}(d*n*ppe)H] (**7**; C$_{36}$H$_{69}$BFeP$_2$, M$_W$ = 631 g/mol): In the glovebox, **2** (20 mg, 0.04 mmol) was weighed into a 20 mL scintillation vial equipped with a stir bar and dissolved in approximately 4 mL of PhCH$_3$. Dicyclohexylborane (HBCy$_2$; 0.04 mmol, 7 mg, 1 equiv.) was added and the solution stirred for 1 h at room temperature. The solution became orange over time. The solvent was removed *in-vacuo* and the product extracted into 3 x 2 mL of pentane and filtered through Celite®. The product was dried *in-vacuo* giving **7** as a yellow oil (23 mg, 81%). **^{1}H NMR (500 MHz, C$_6$D$_6$, 298 K):** δ_H = 2.42 (s; 2H, η^5-C$_5$Me$_4$–C<u>H</u>$_2$–B(Cy$_2$)), 2.00 (s; 6H, η^5-C$_5$<u>Me</u>$_4$–CH$_2$–B(Cy$_2$)), 1.97 (s; 6H, η^5-C$_5$<u>Me</u>$_4$–CH$_2$–B(Cy$_2$)), 1.78-1.76 (10H, multiple overlapping C<u>H</u>$_2$/C<u>H</u> signals), 1.61-1.58 (10H, multiple overlapping C<u>H</u>$_2$/C<u>H</u> signals), 1.48-1.46 (5H, multiple overlapping C<u>H</u>$_2$/C<u>H</u> signals), 1.30 (17H; multiple overlapping C<u>H</u>$_2$/C<u>H</u> signals), 1.08-1.02 (12H, multiple overlapping P-CH$_2$-CH$_2$-C<u>H</u>$_3$ signals), -17.83 (t; 1H, [Fe]–<u>H</u> ($^{2}J_{H-P}$ = 70.6 Hz). **^{13}C{^{1}H} NMR (125.8 MHz, C$_6$D$_6$, 298 K):** δ_C = 90.0 (s; η^5-<u>C</u>$_5$Me$_4$–

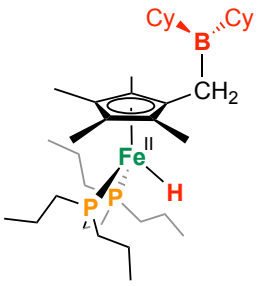

CH_2–B(Cy_2)), 83.7 (s; η^5-$\underline{C}_5Me_4$−CH_2–B(Cy_2)), 82.7 (s; η^5-$\underline{C}_5Me_4$−CH_2–B(Cy_2)), 35.9-35.7 (multiple overlapping sp^3-carbon signals), 27.8-27.2 (multiple overlapping sp^3-carbon signals), 26.5 (br. s; η^5-C_5Me_4−$\underline{C}H_2$–B(Cy_2)), 19.2 (br. s; sp^3-carbon signal), 18.7 (br. s; sp^3-carbon signal), 16.8 (br. s; P-CH_2-CH_2-$\underline{C}H_3$), 16.6 (br. s; P-CH_2-CH_2-$\underline{C}H_3$), 13.7 (s; η^5-$C_5\underline{Me}_4$−CH_2–B(Cy_2)), 13.1 (s; η^5-$C_5\underline{Me}_4$−CH_2–B(Cy_2)). **$^{31}P\{^1H\}$ NMR (202.5 MHz, C_6D_6, 298 K):** δ_P = +97.8. **$^{11}B\{^1H\}$ NMR (160.5 MHz, C_6D_6, 298 K):** δ_B = +82.6 ($\Delta_{1/2}$ = 1390 Hz). **FT-IR (ATR):** 1844 cm^{-1} (ν[Fe–H]).

Multinuclear NMR Data:

Figure S1: 1, ^{1}H NMR, d$_8$-THF, 500 MHz, 298 K.

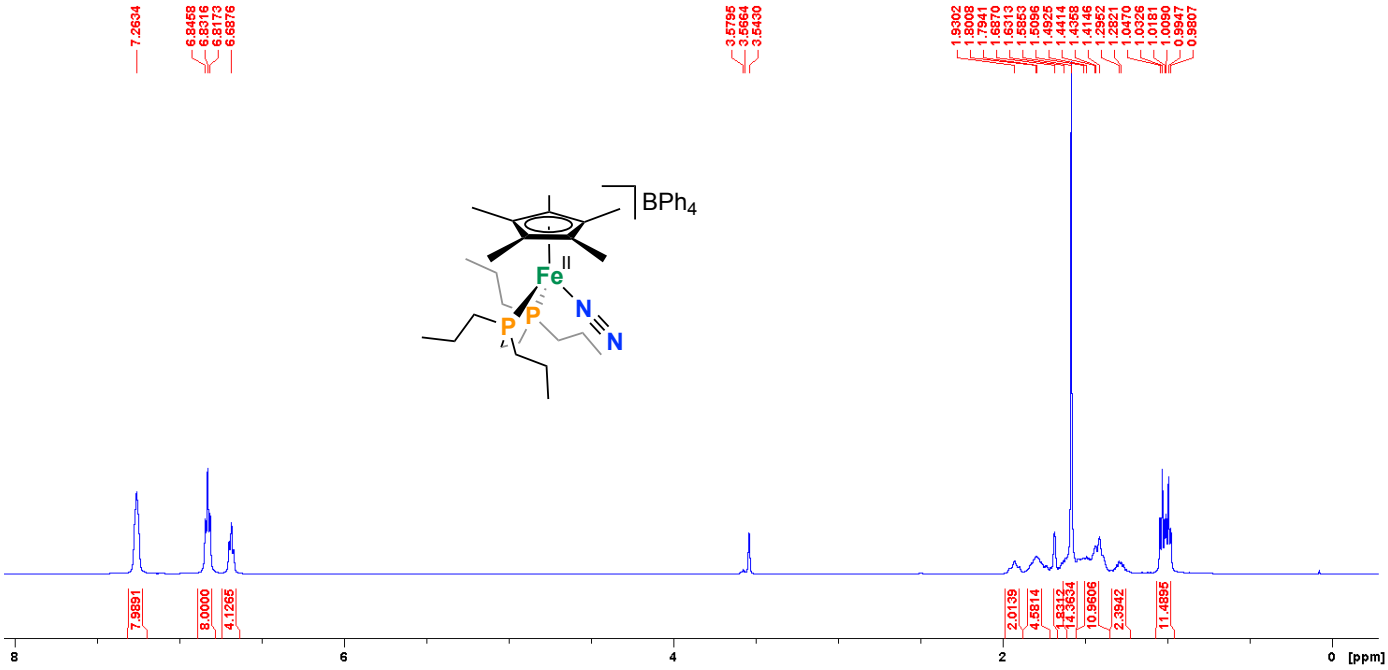

Figure S2: 1, ^{1}H NMR, d$_8$-THF, 500 MHz, 298 K – expansion of the alkyl region.

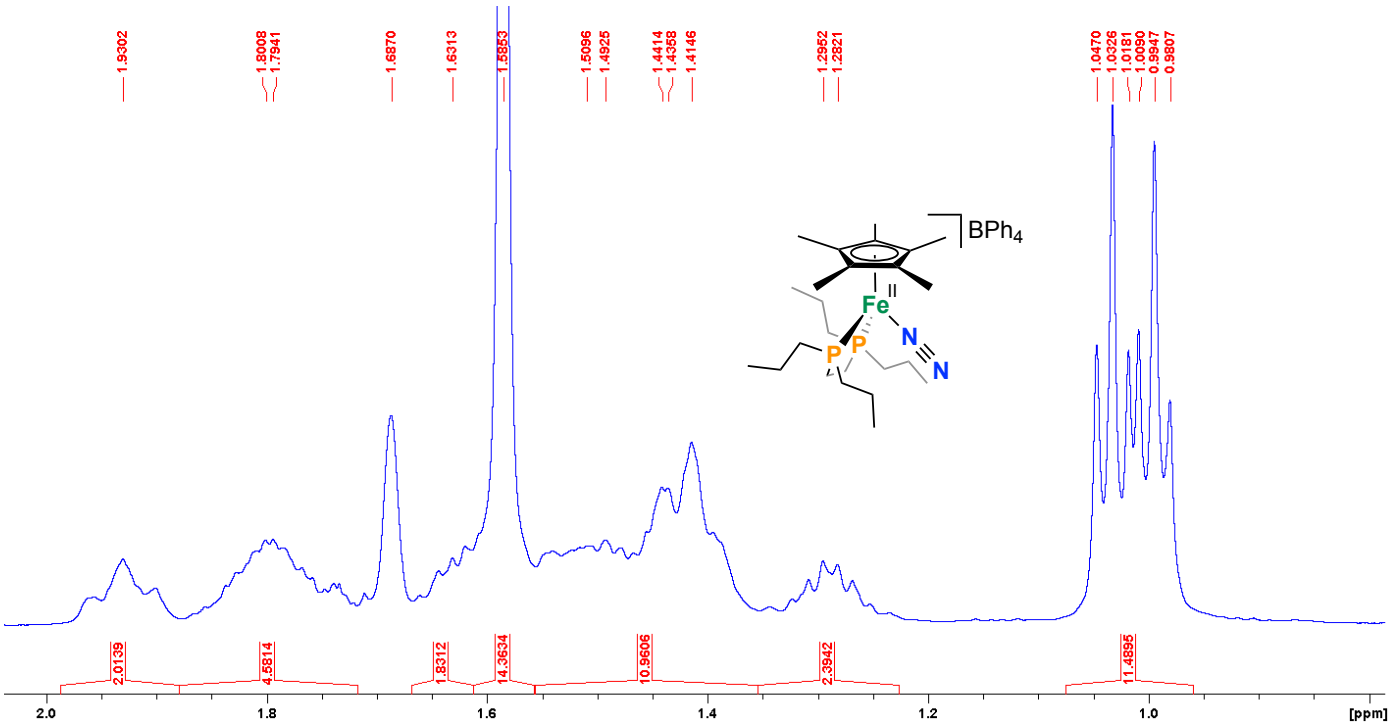

Figure S3: 1, $^{31}P\{^{1}H\}$ NMR, d_8-THF, 202.5 MHz, 298 K.

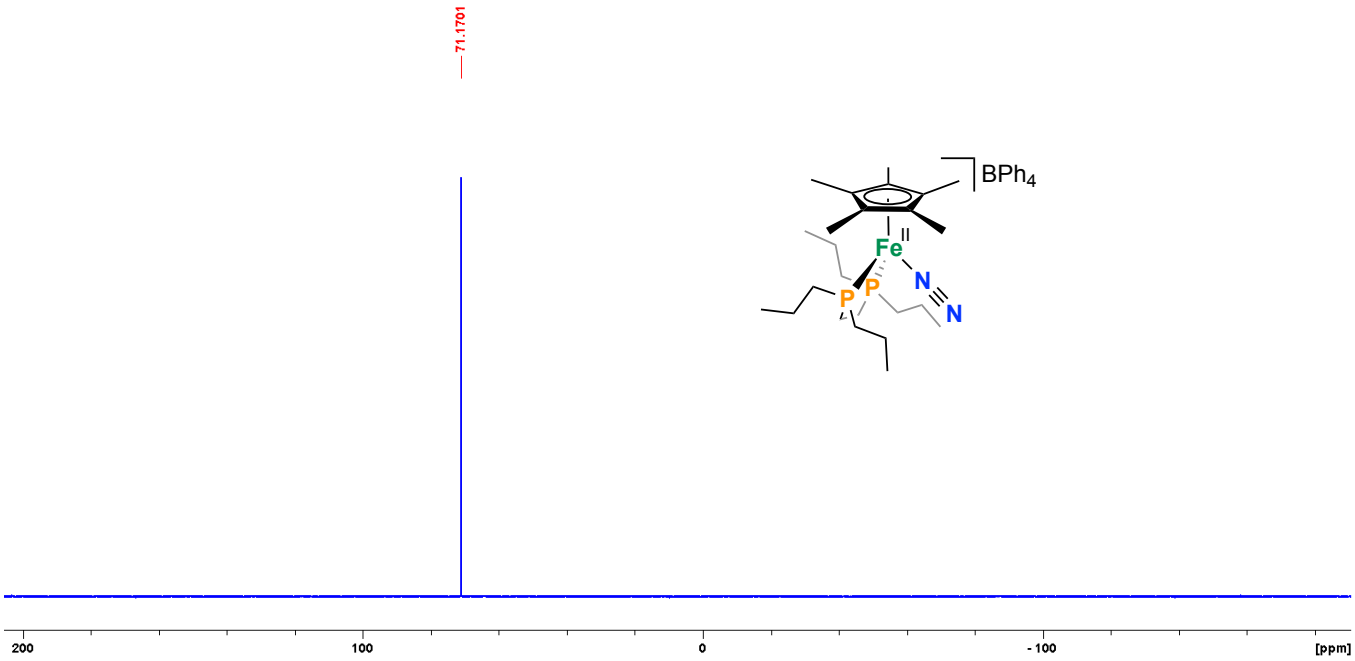

Figure S4: 1, $^{13}C\{^{1}H\}$ NMR, d_8-THF, 125.8 MHz, 298 K.

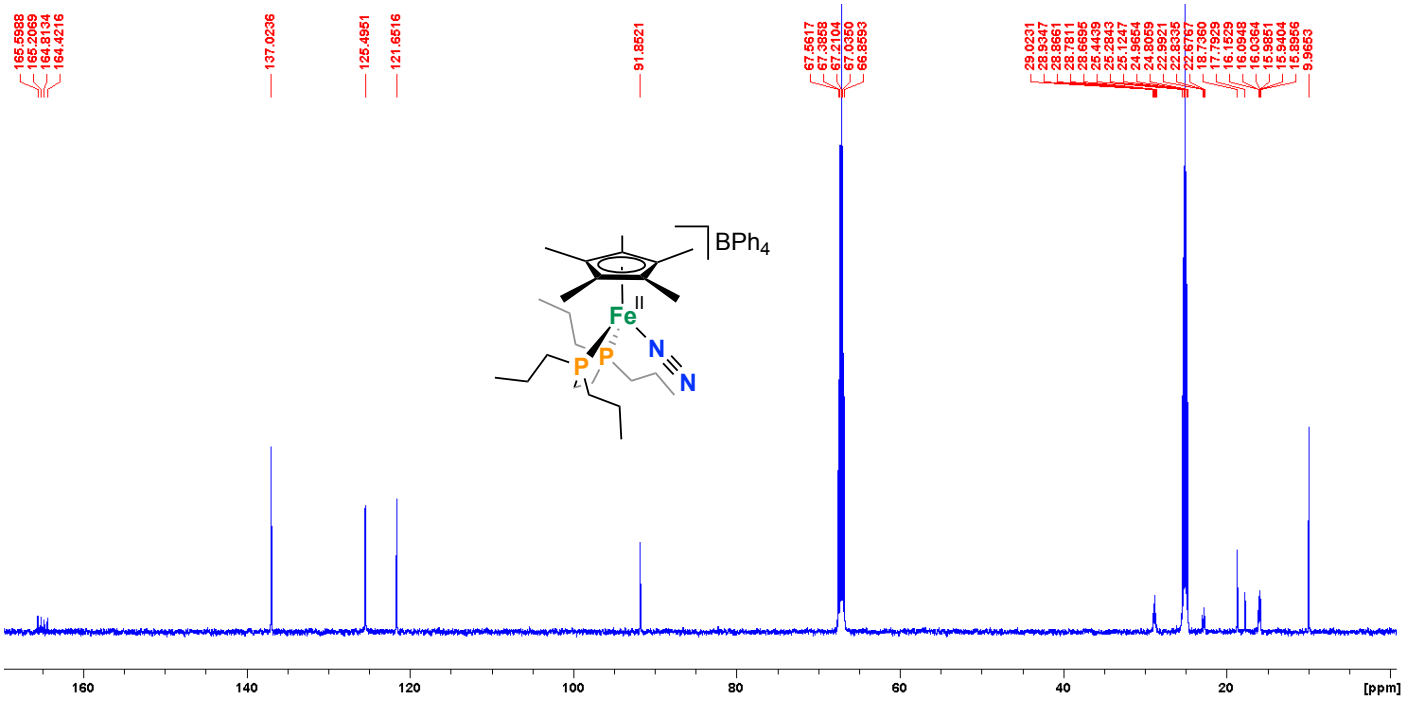

Figure S5: 1, $^{11}B\{^{1}H\}$ NMR, d_8-THF, 160.5 MHz, 298 K.

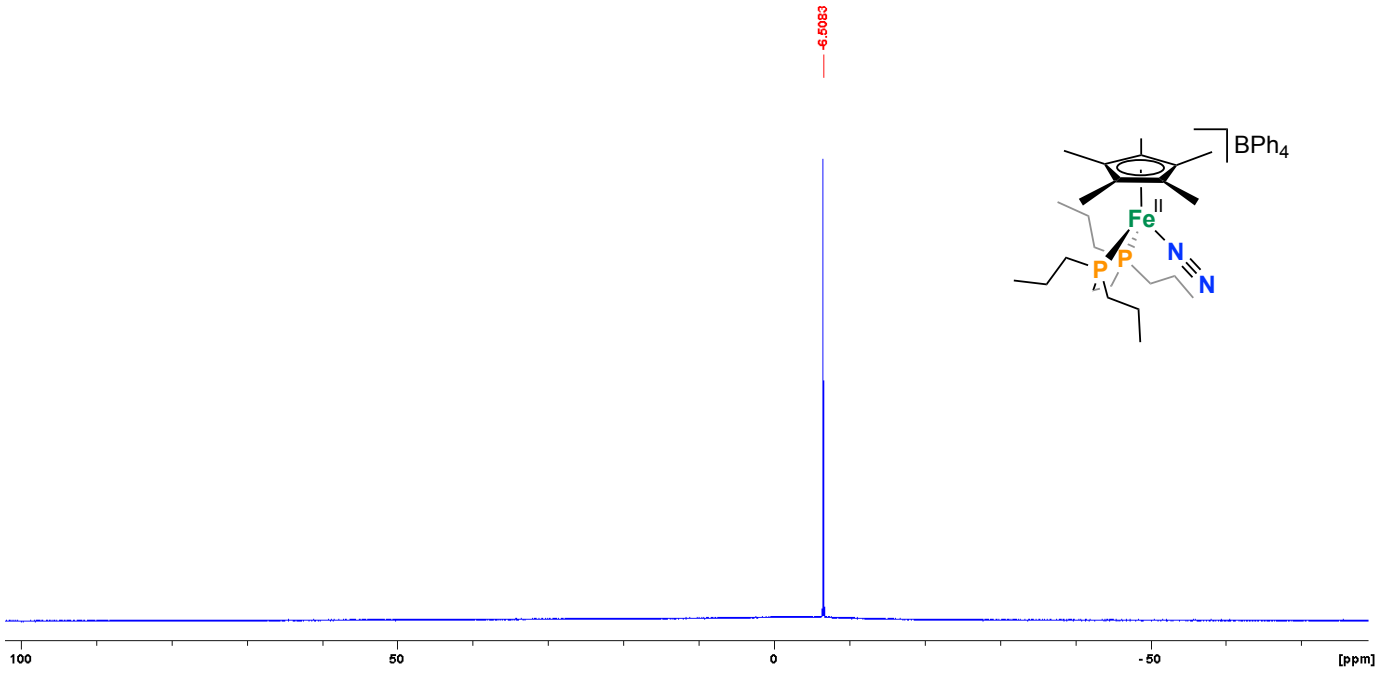

Figure S6: 1, FT-IR ATR, 298 K ($\nu[N_2]$ = 2098 cm^{-1}).

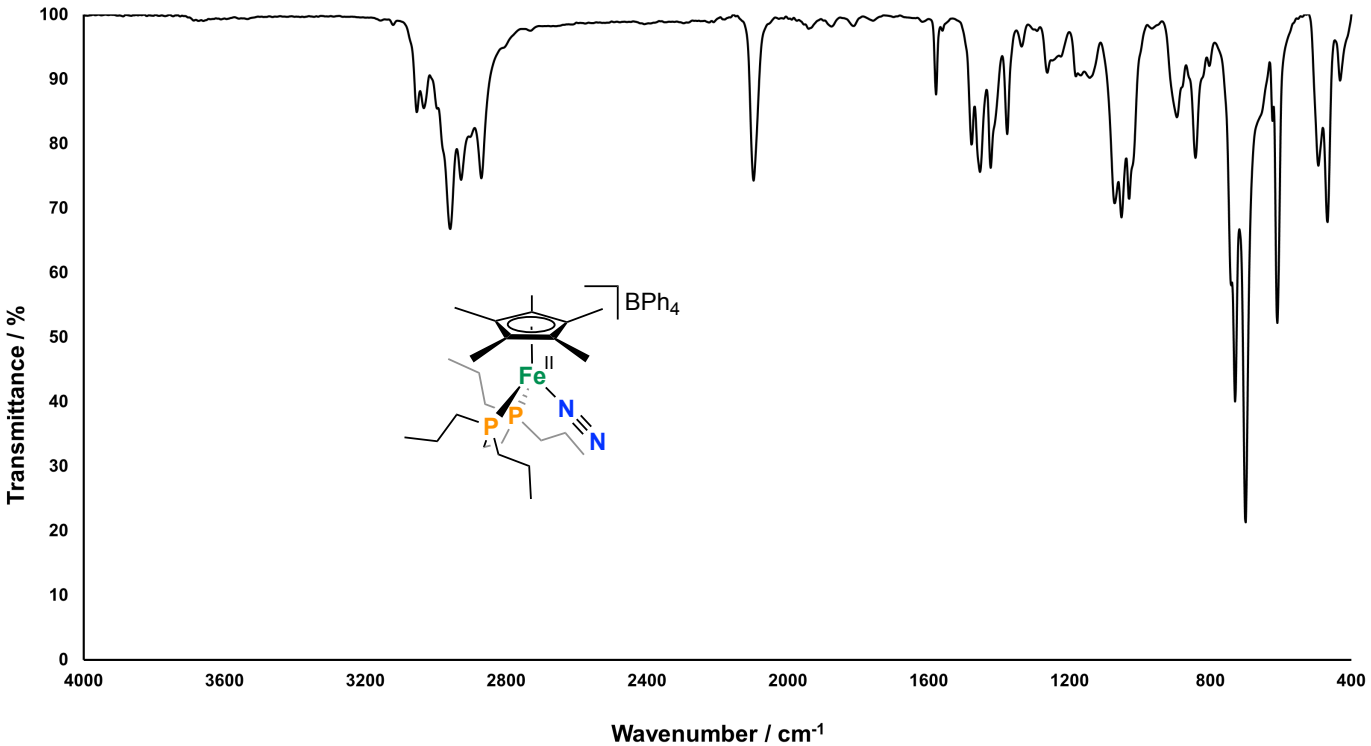

Figure S7: 2, ^{1}H NMR, C_6D_6, 500 MHz, 298 K.

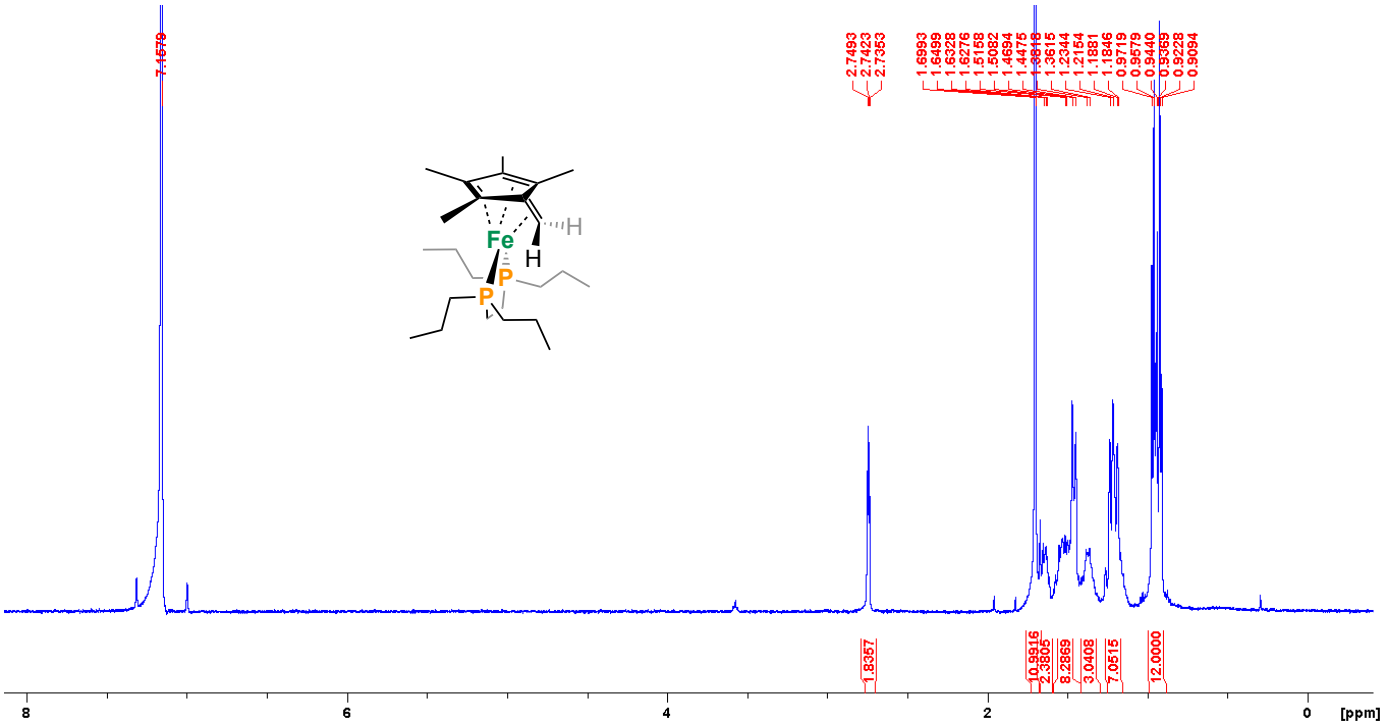

Figure S8: 2, ^{1}H NMR, C_6D_6, 500 MHz, 298 K – expansion of the alkyl region.

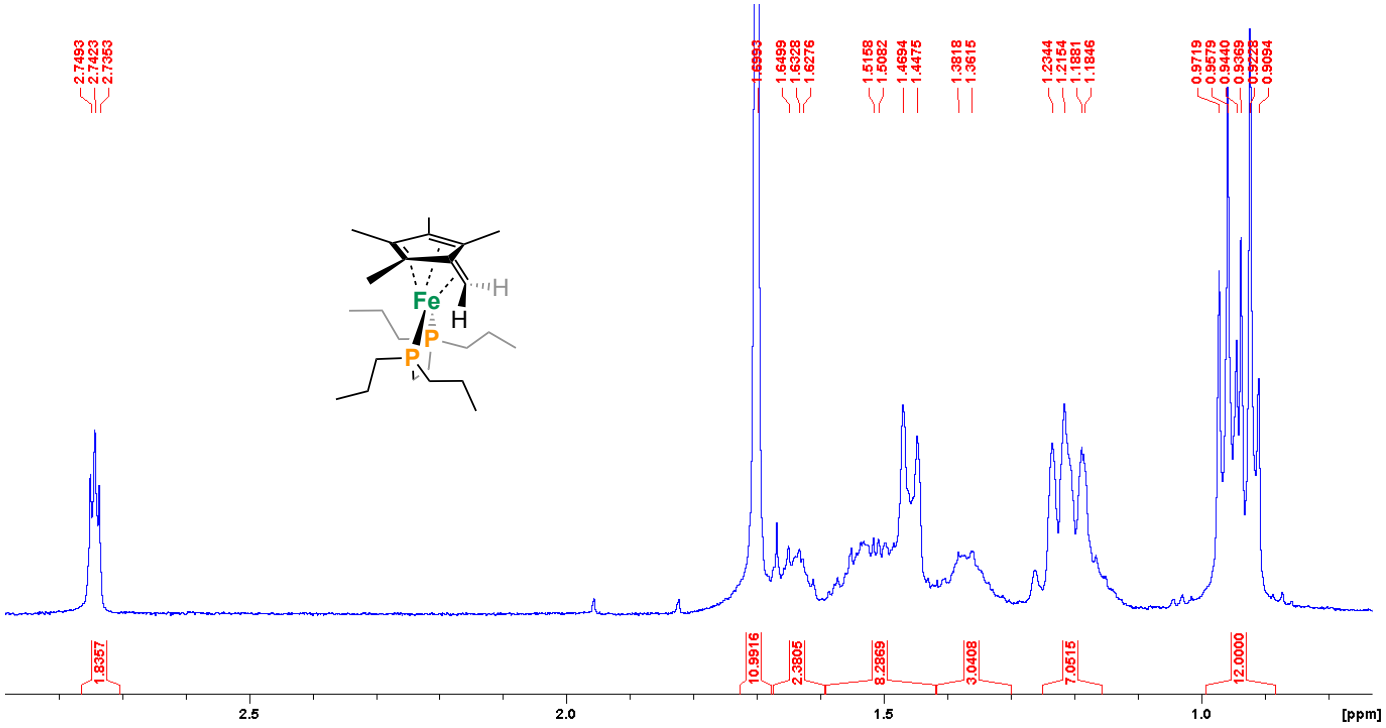

Figure S9: 2, $^{31}P\{^{1}H\}$ NMR, C_6D_6, 202.5 MHz, 298 K.

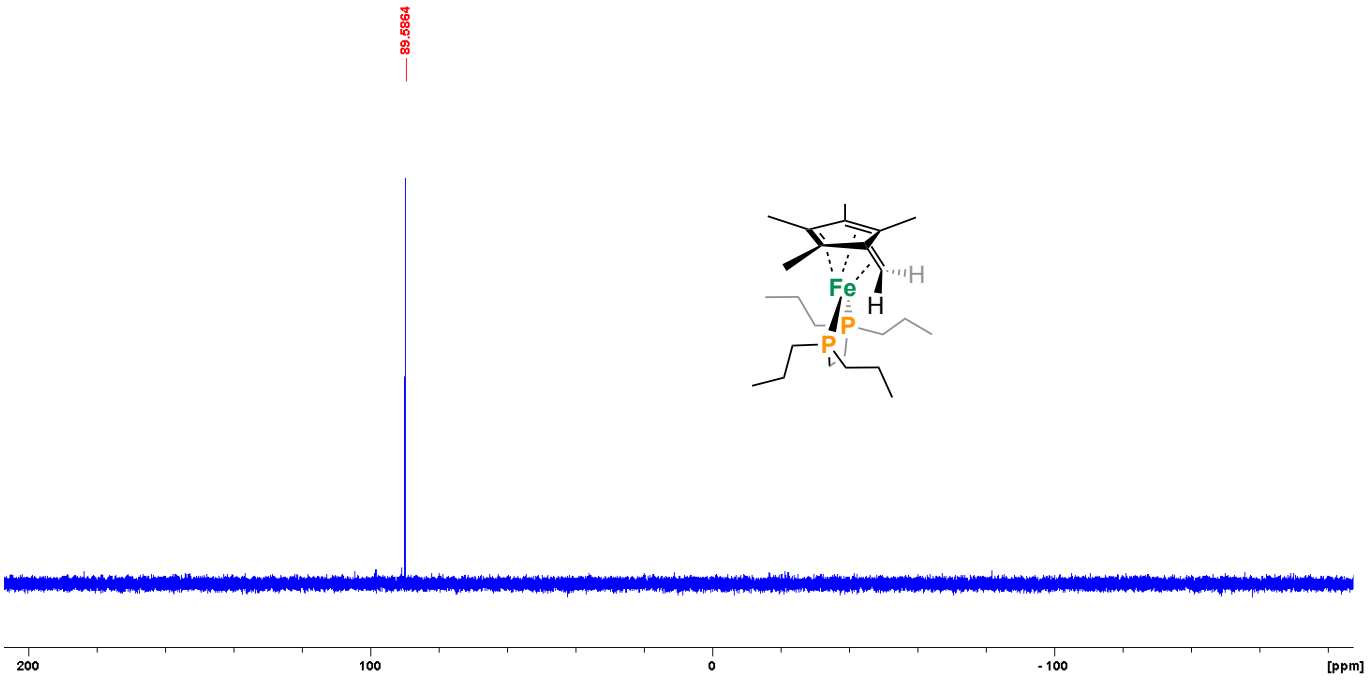

Figure S10: 2, $^{13}C\{^{1}H\}$ NMR, C_6D_6, 75.5 MHz, 298 K.

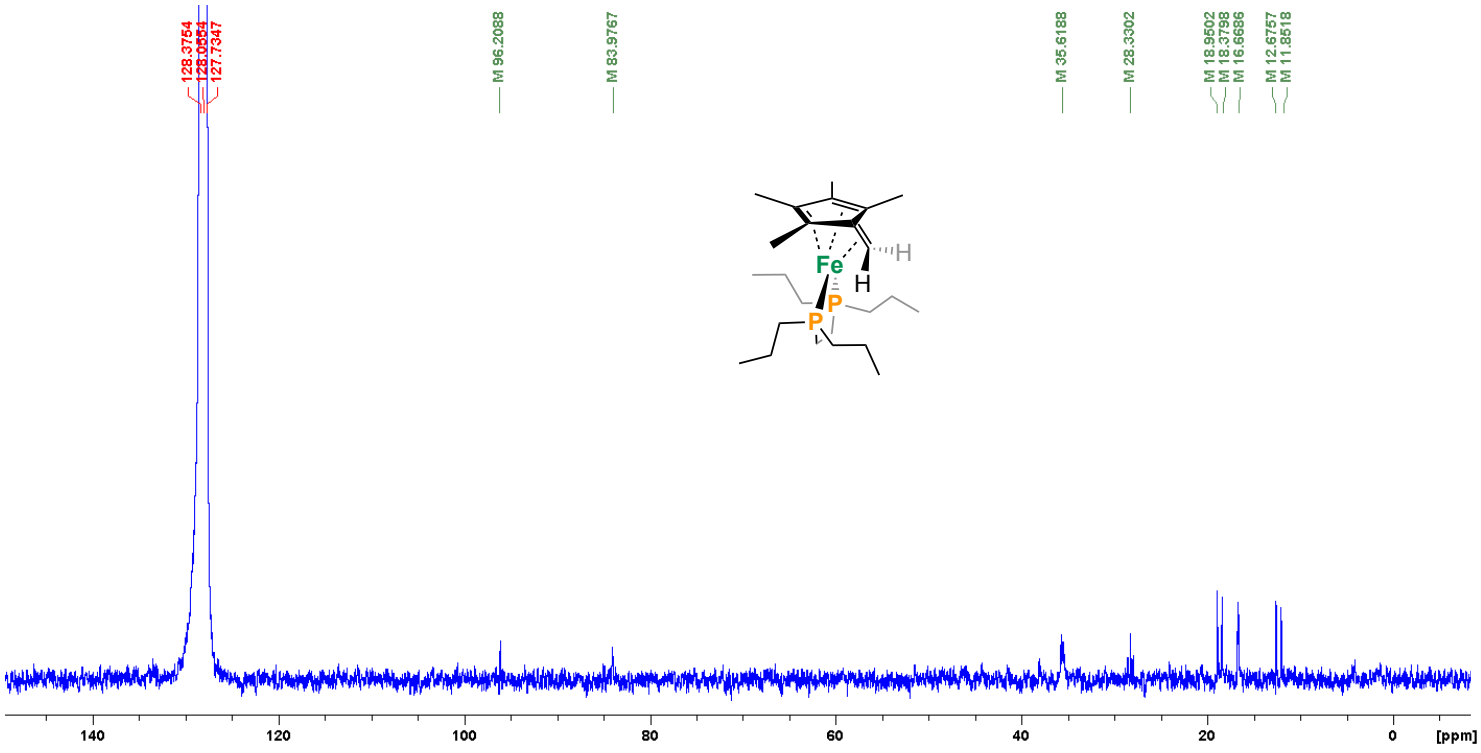

Figure S11: 3, ^{1}H NMR, C_6D_6, 500 MHz, 298 K.

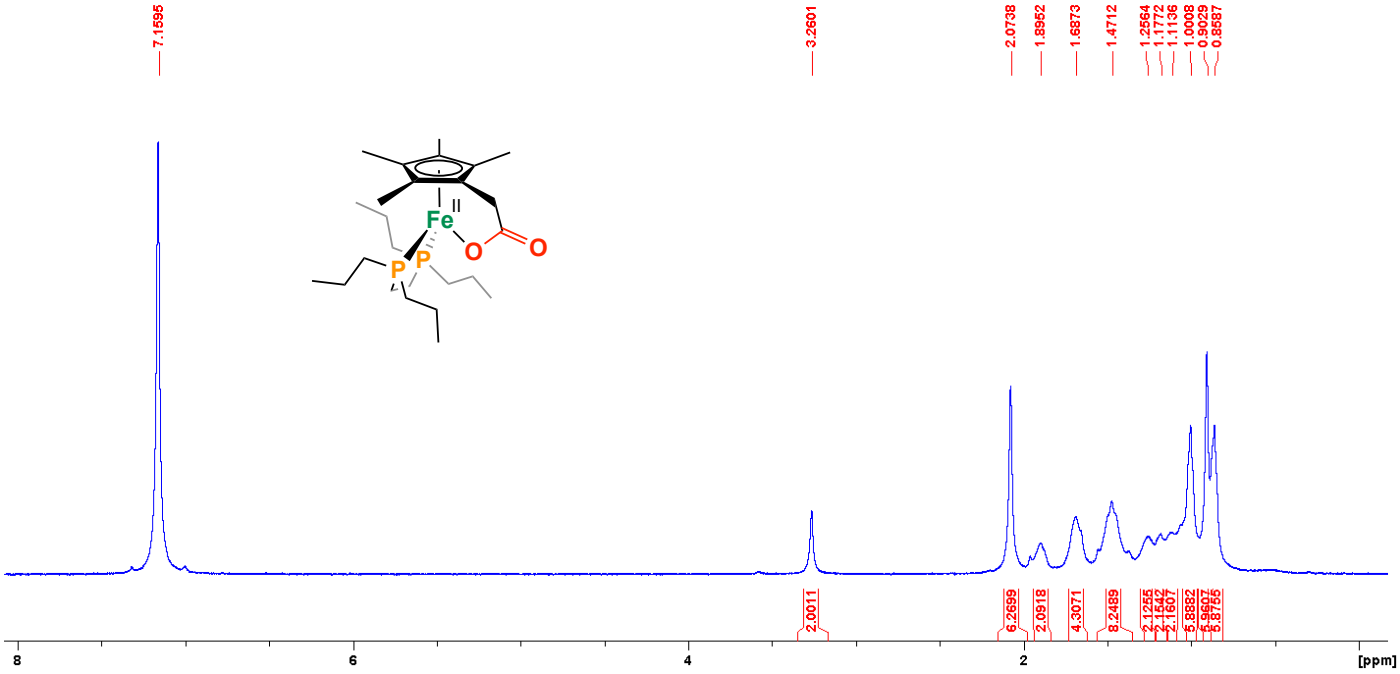

Figure S12: 3, $^{31}P\{^{1}H\}$ NMR, C_6D_6, 121.5 MHz, 298 K.

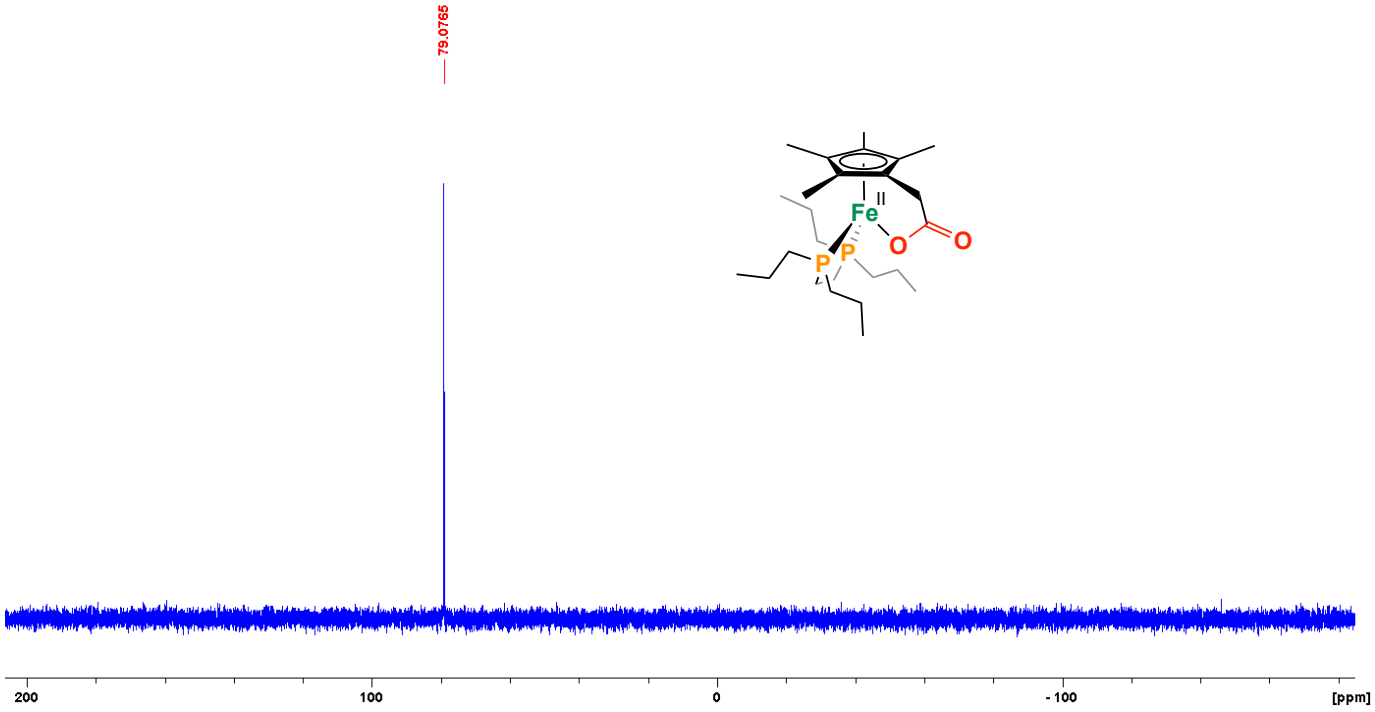

Figure S13: 3, $^{13}C\{^{1}H\}$ NMR, C_6D_6, 125.8 MHz, 298 K.

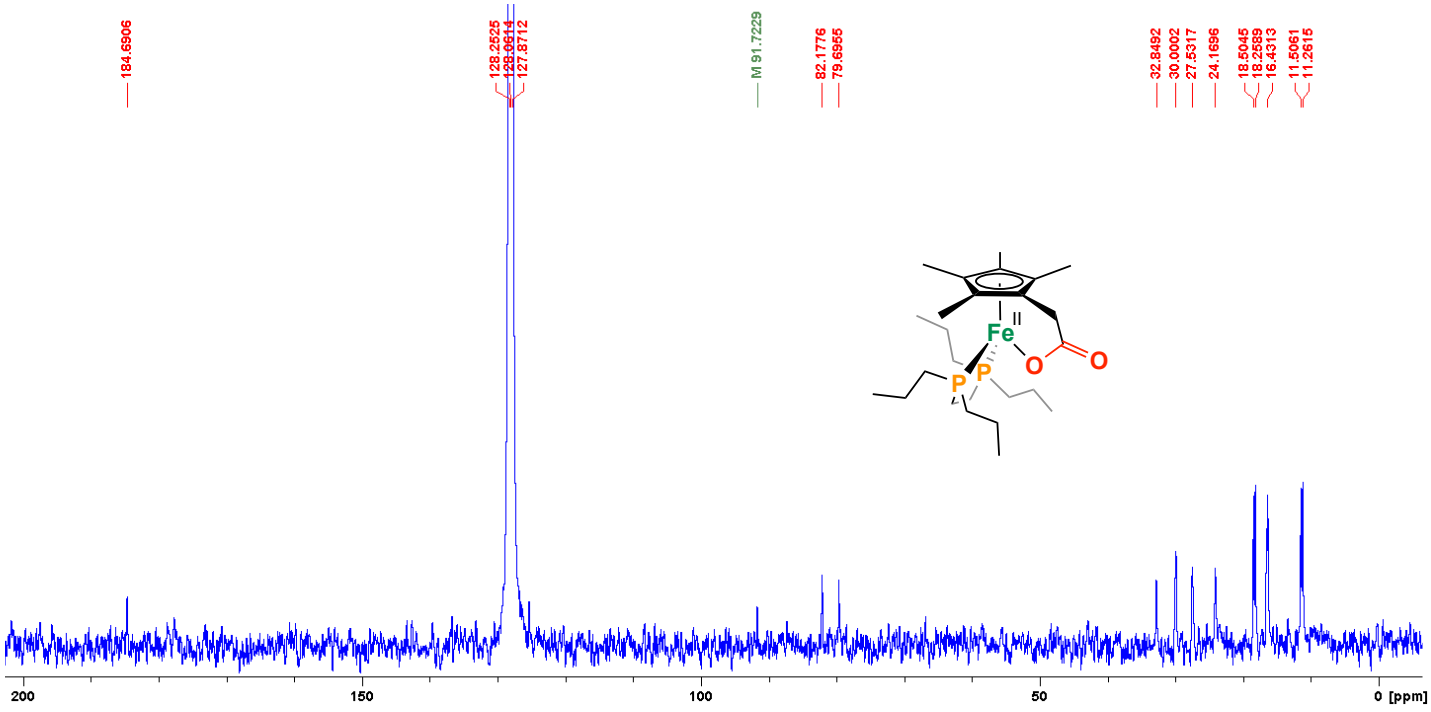

Figure S14: 3, ^{1}H-^{13}C HMBC NMR showing the location of the η^5-C_5Me_4–CH_2–$\underline{C}O_2$ signal from the proton signal for η^5-C_5Me_4–$C\underline{H}_2$–CO_2.

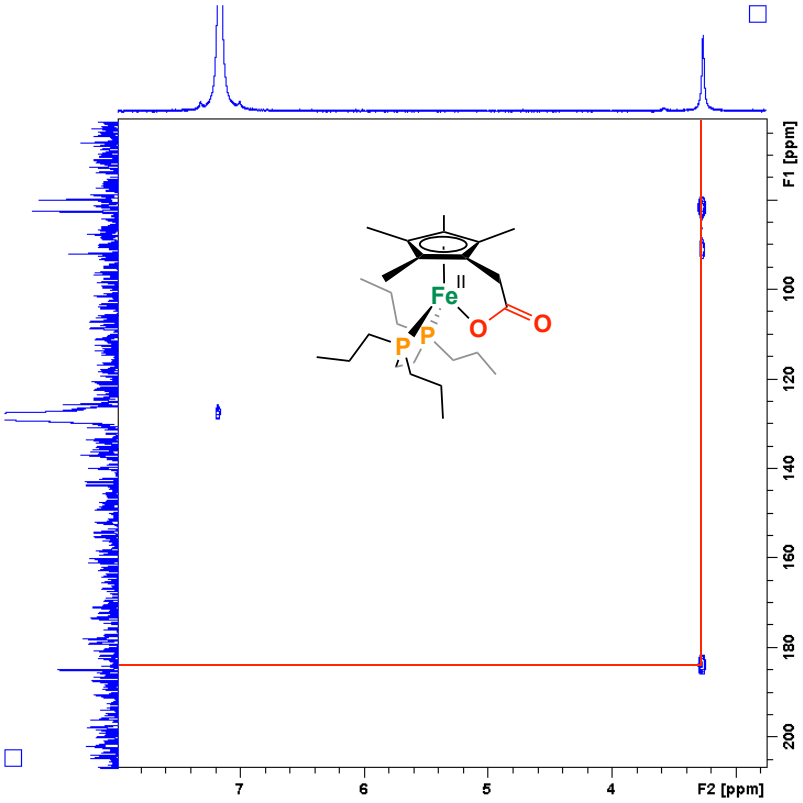

Figure S15: 3, FT-IR ATR, 298 K (ν[C=O] = 1622 cm^{-1}).

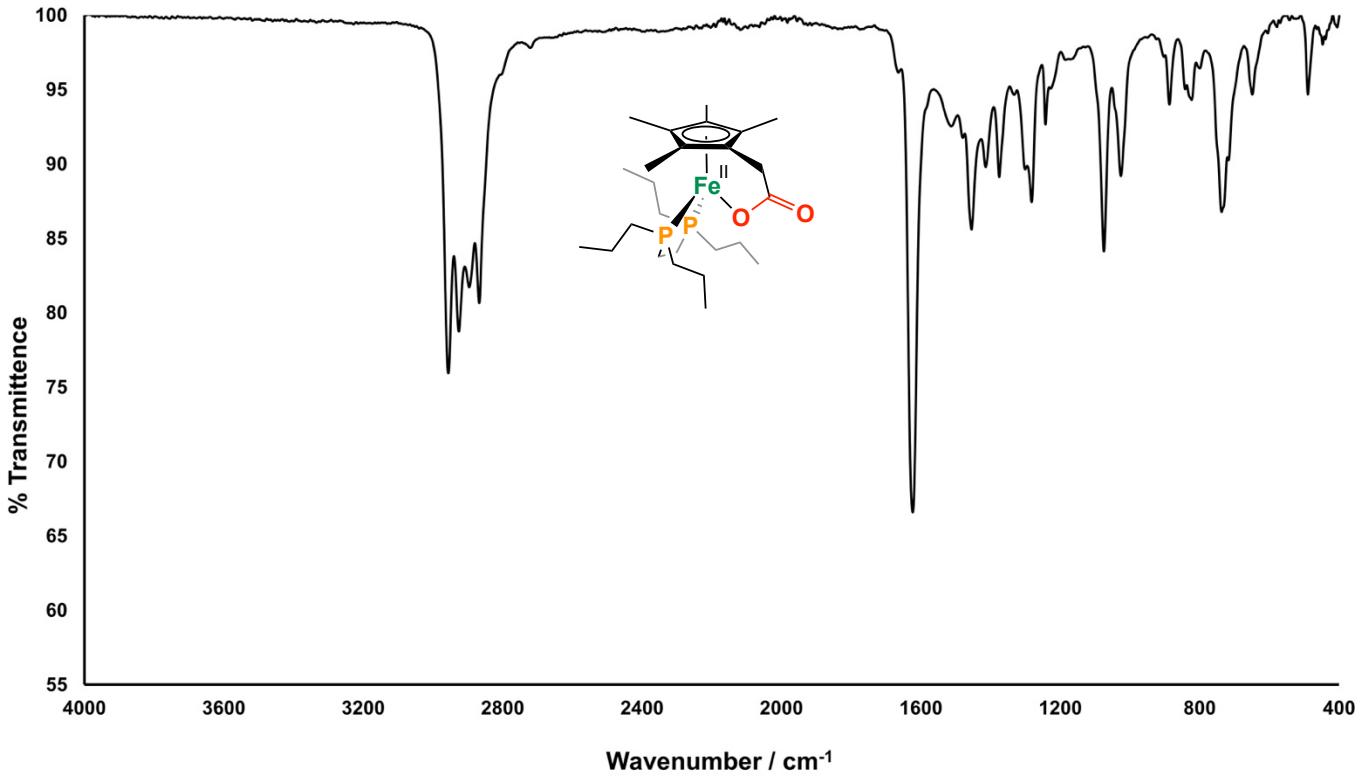

Figure S16: 4, ^{1}H NMR, C_6D_6, 300 MHz, 298 K.

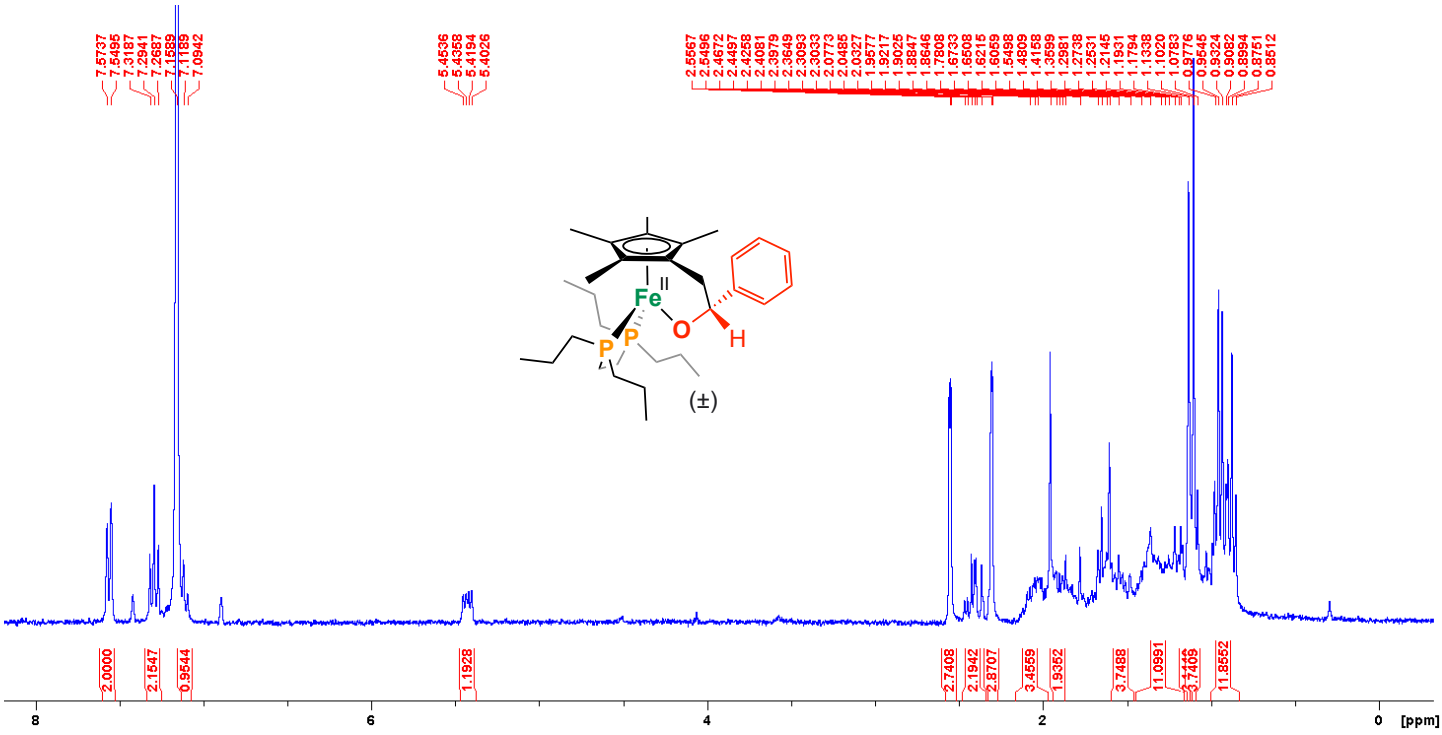

Figure S17: 4, $^{31}P\{^{1}H\}$ NMR, C_6D_6, 121.5 MHz, 298 K. Insert shows an enhanced view of the two sets of doublets.

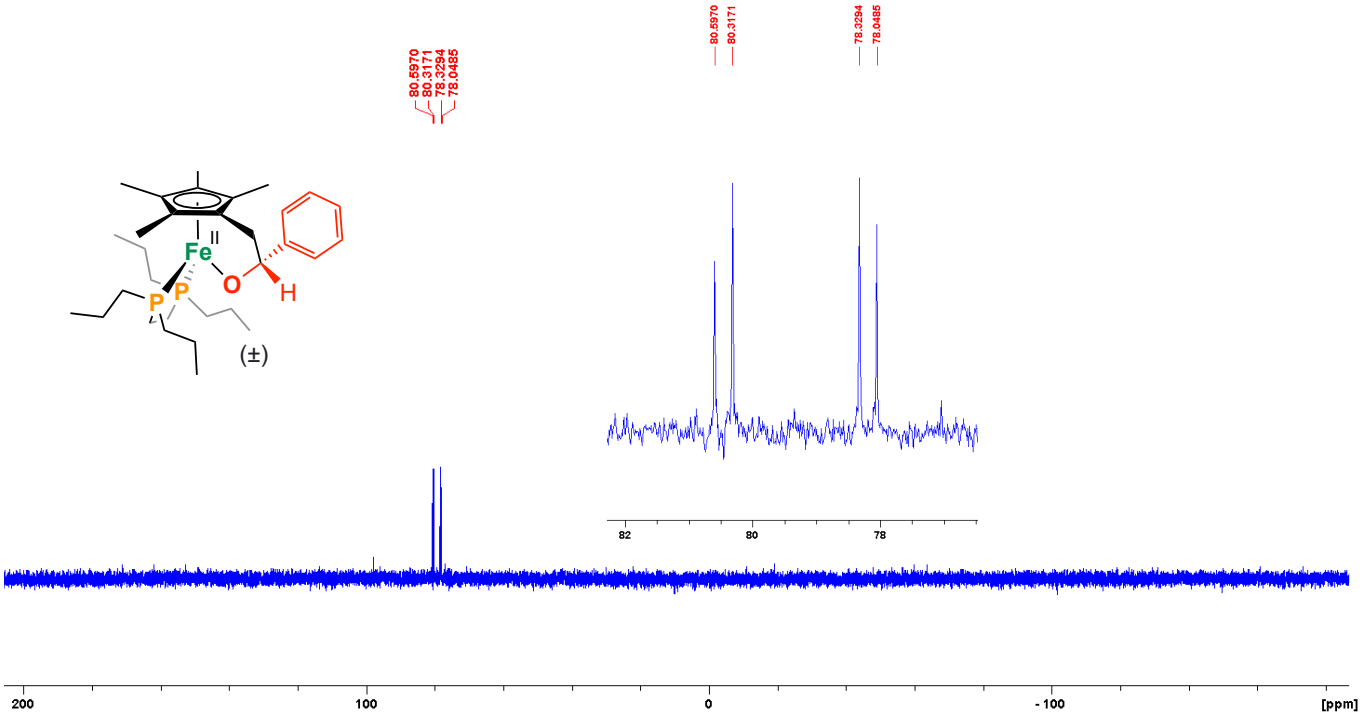

Figure S18: 4, $^{13}C\{^{1}H\}$ NMR, C_6D_6, 75.5 MHz, 298 K.

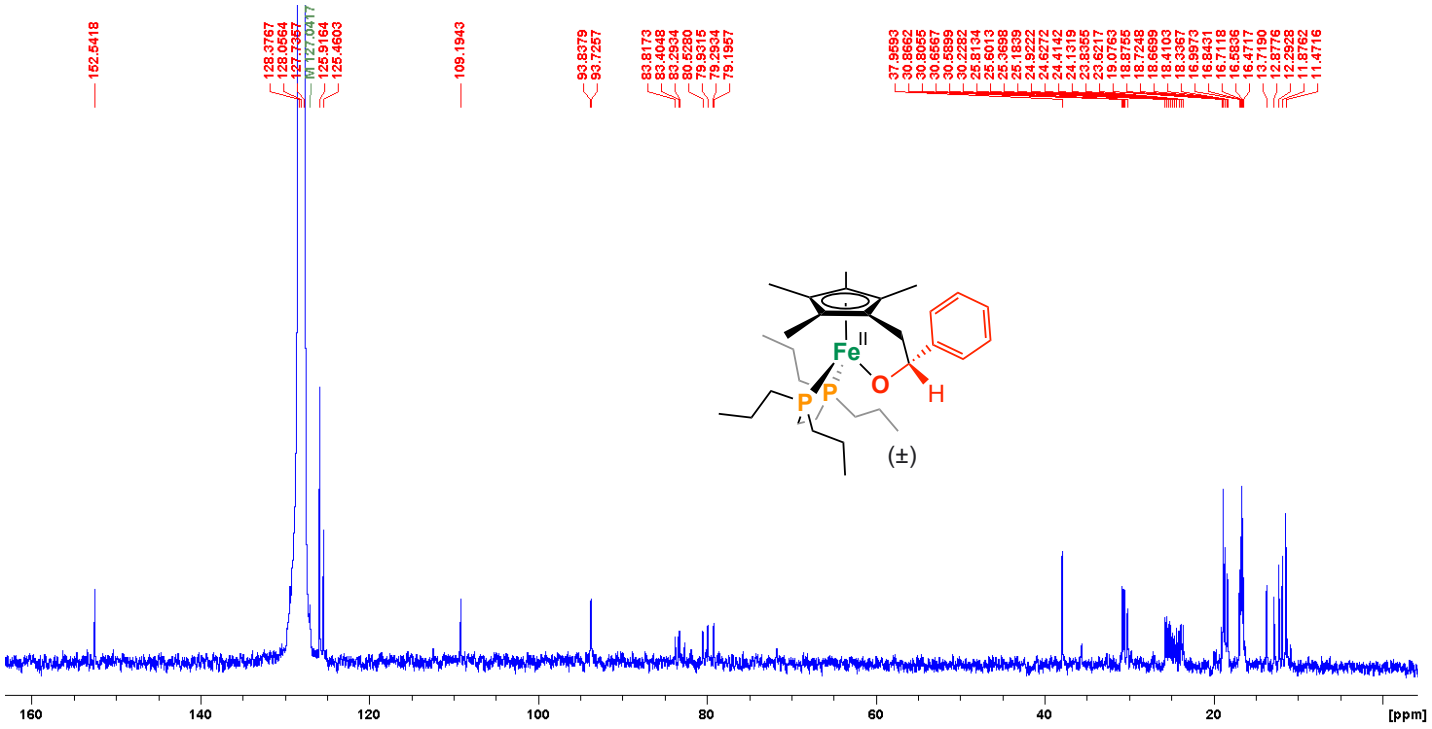

Figure S19: 5, ^{1}H NMR, d_8-toluene, 300 MHz, 298 K.

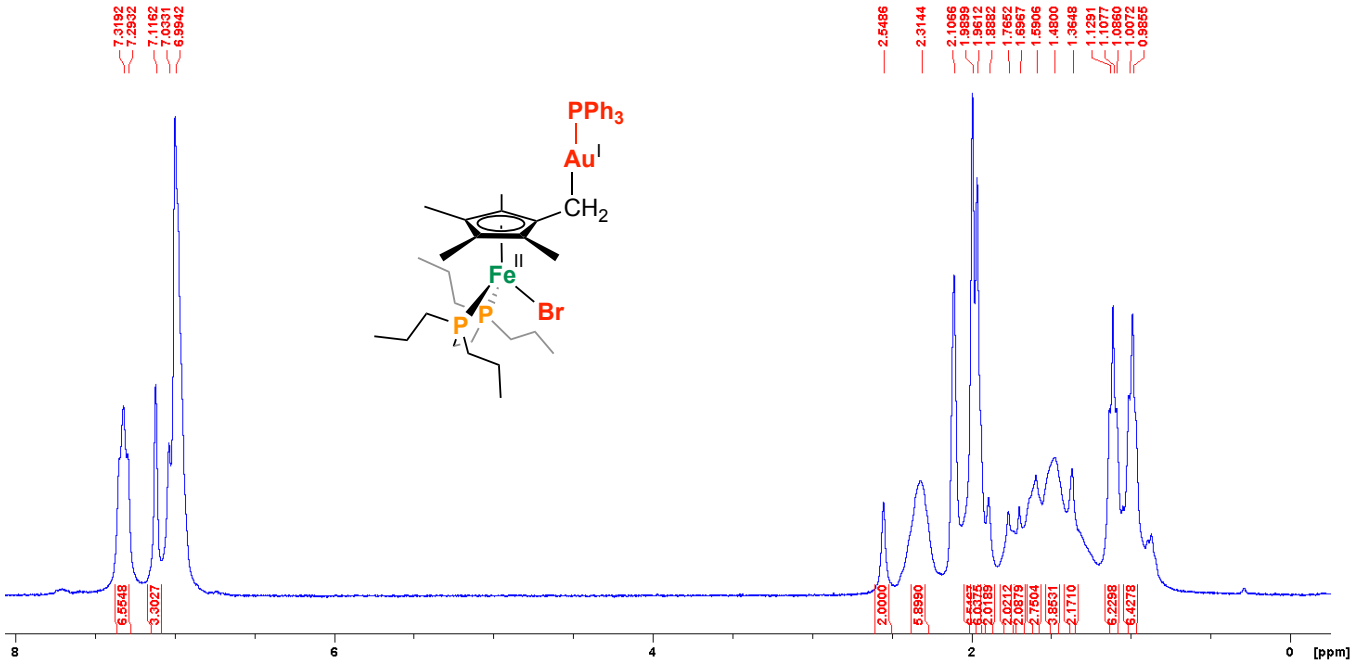

Figure S20: 5, $^{31}P\{^{1}H\}$ NMR, d_8-toluene, 202.5 MHz, 298 K.

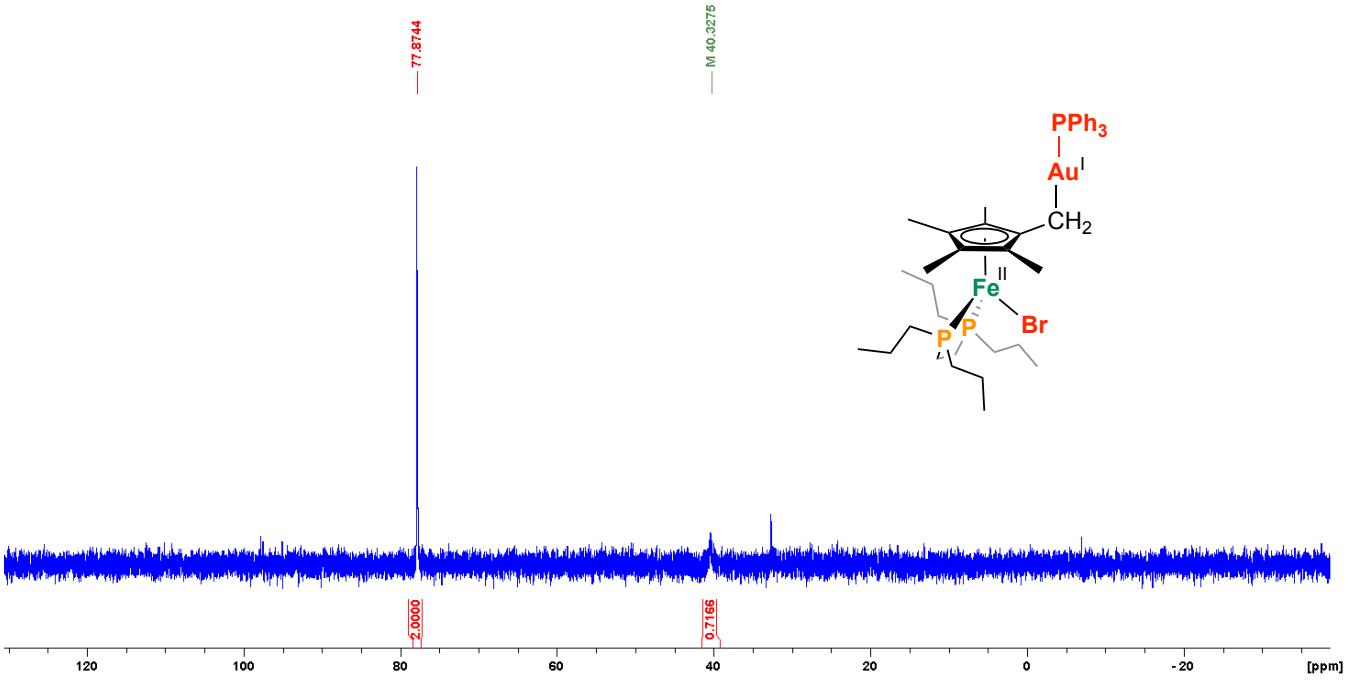

Figure S21: 5, $^{13}C\{^{1}H\}$ NMR, d_8-toluene, 125.8 MHz, 298 K.

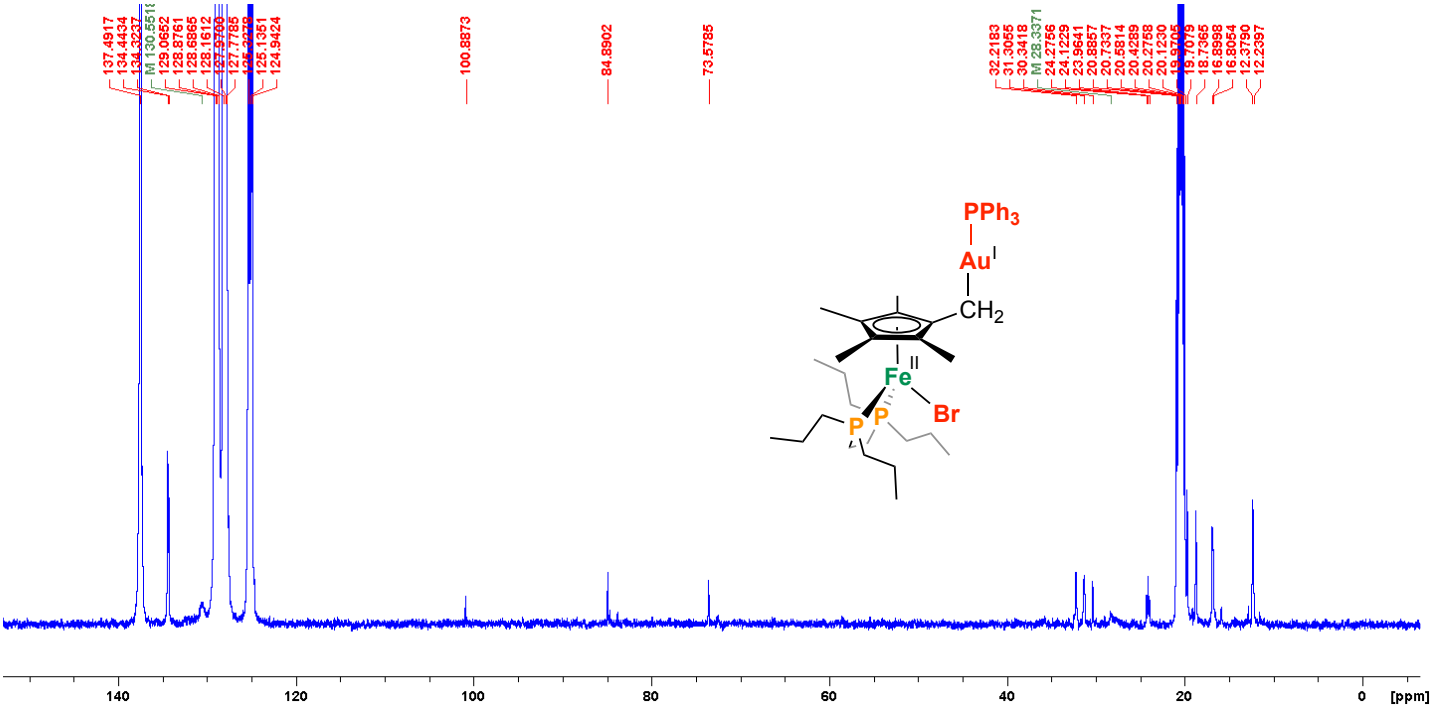

Figure S22: 5, ^{1}H-^{13}C HSQC showing the location of the η^5-C_5Me_4–$\underline{C}H_2$– Au–PPh_3 carbon signal from the proton signal for η^5-C_5Me_4–$C\underline{H}_2$–Au–PPh_3.

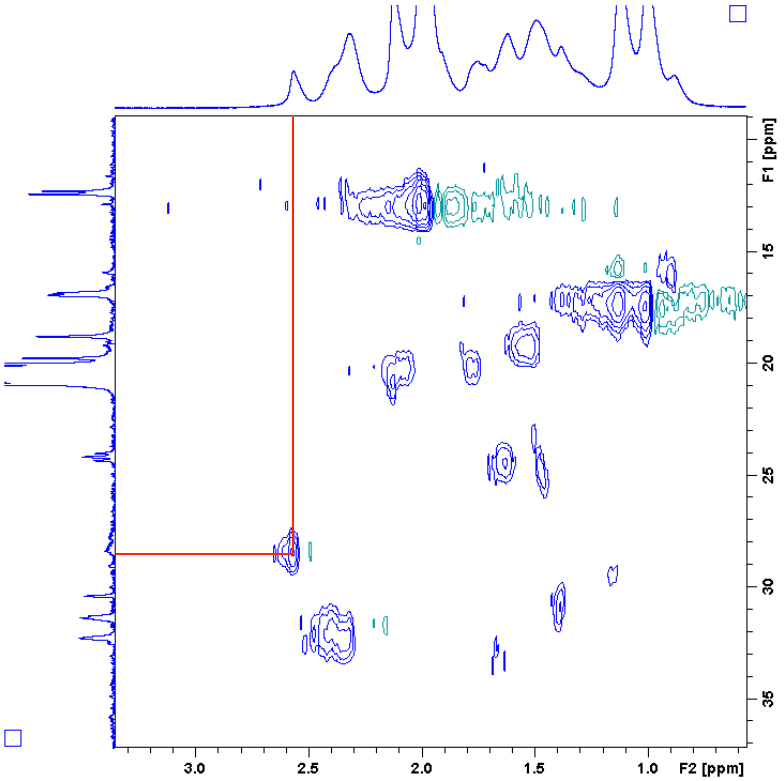

Figure S23: 6, ^{1}H NMR, d_8-THF, 300 MHz, 298 K

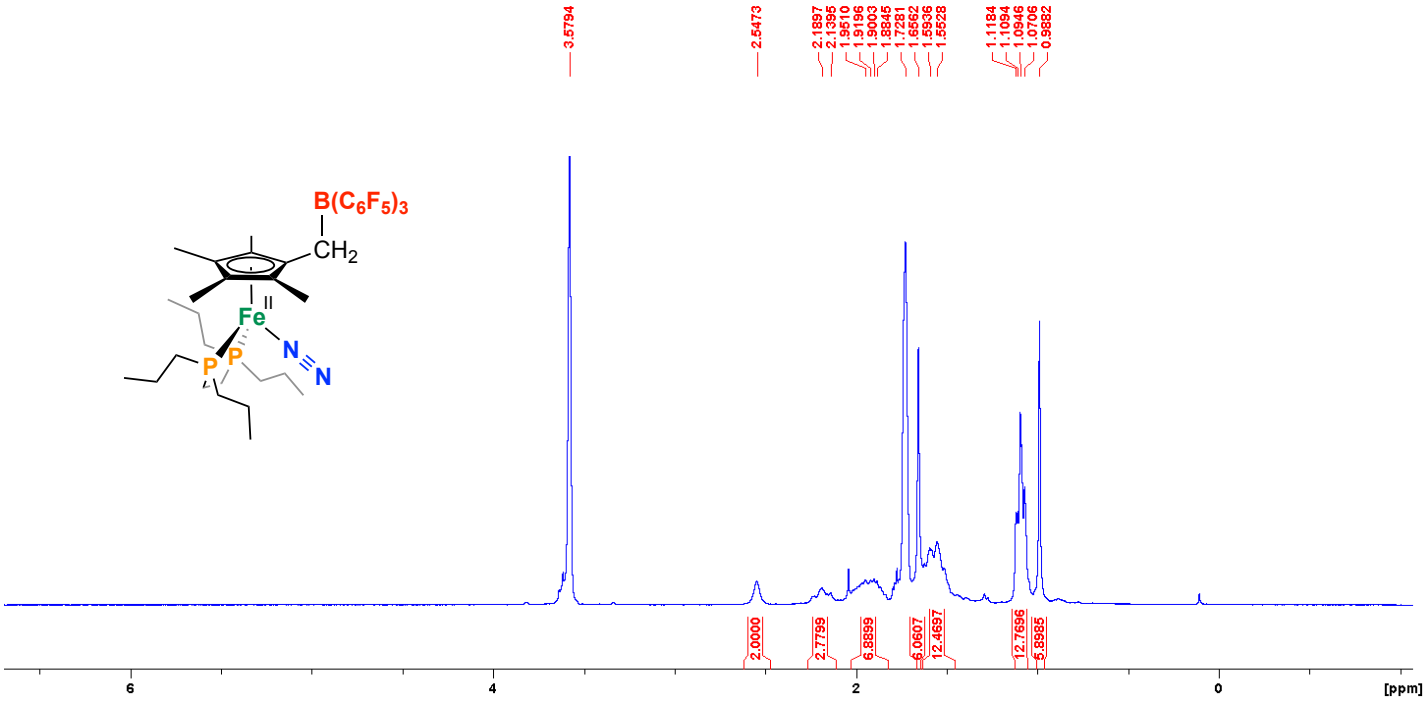

Figure S24: 6, $^{31}P\{^{1}H\}$ NMR, d_8-THF, 202.5 MHz, 298 K.

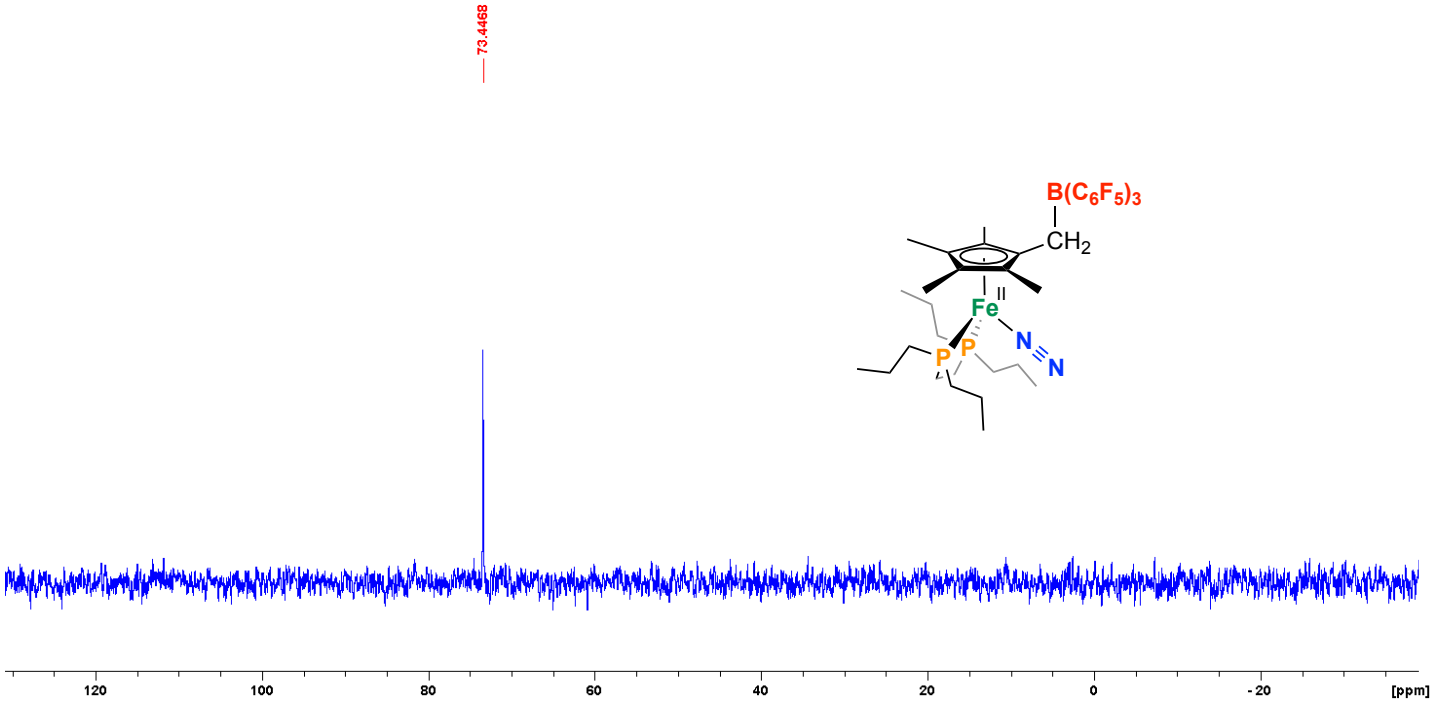

Figure S25: 6, $^{11}B\{^{1}H\}$ NMR, d8-THF, 96.3 MHz, 298 K.

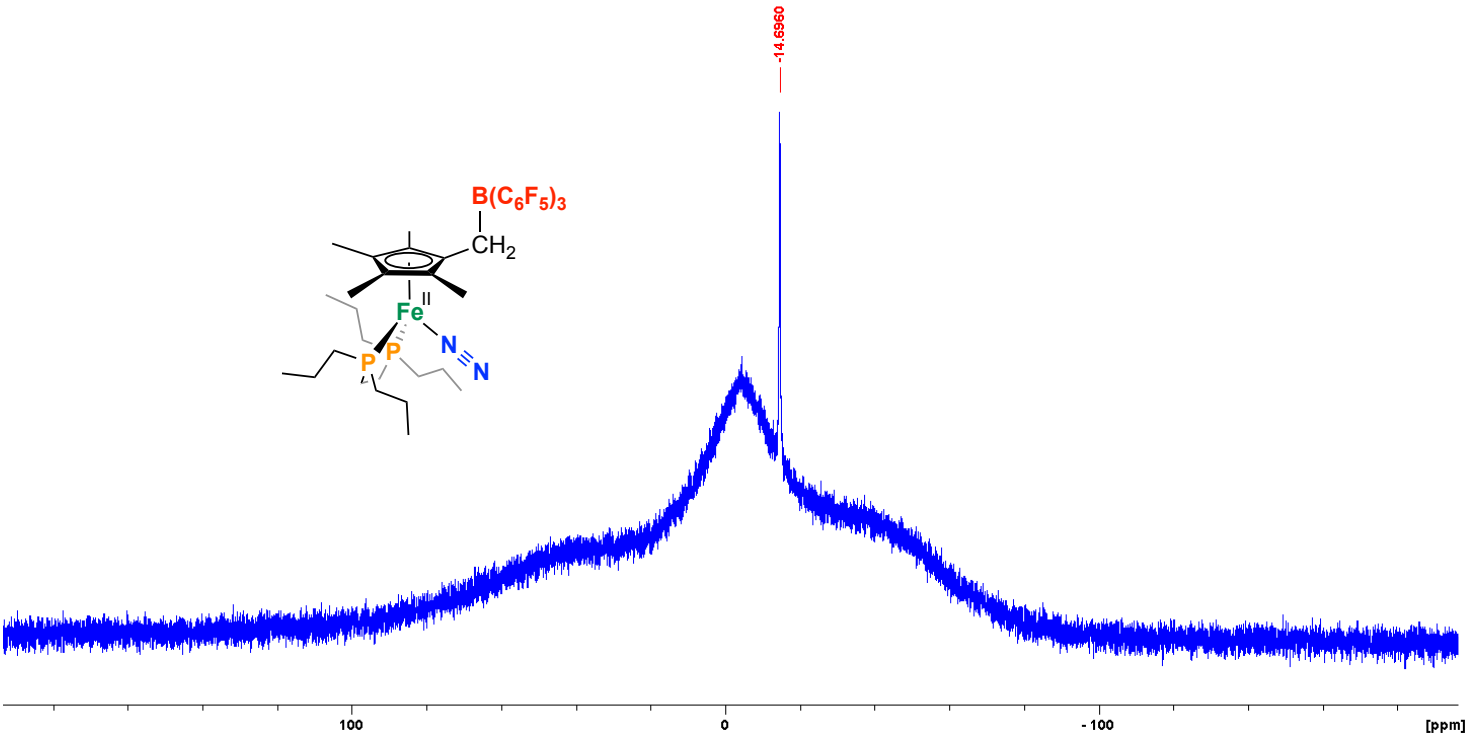

Figure S26: 6, $^{19}F\{^{1}H\}$ NMR, d8-THF, 282.4 MHz, 298 K.

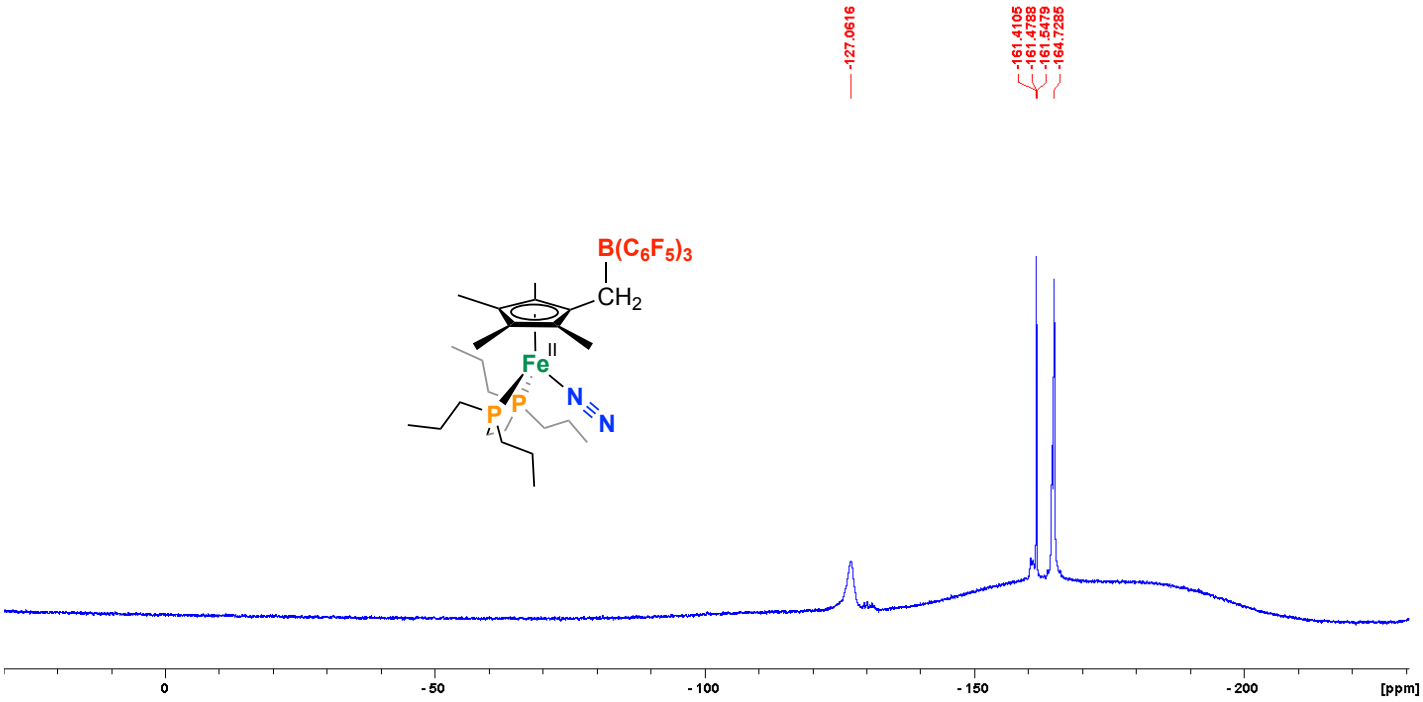

Figure S27: 6, $^{13}C\{^{1}H\}$ NMR, THF-d_8, 125.8 MHz, 298 K.

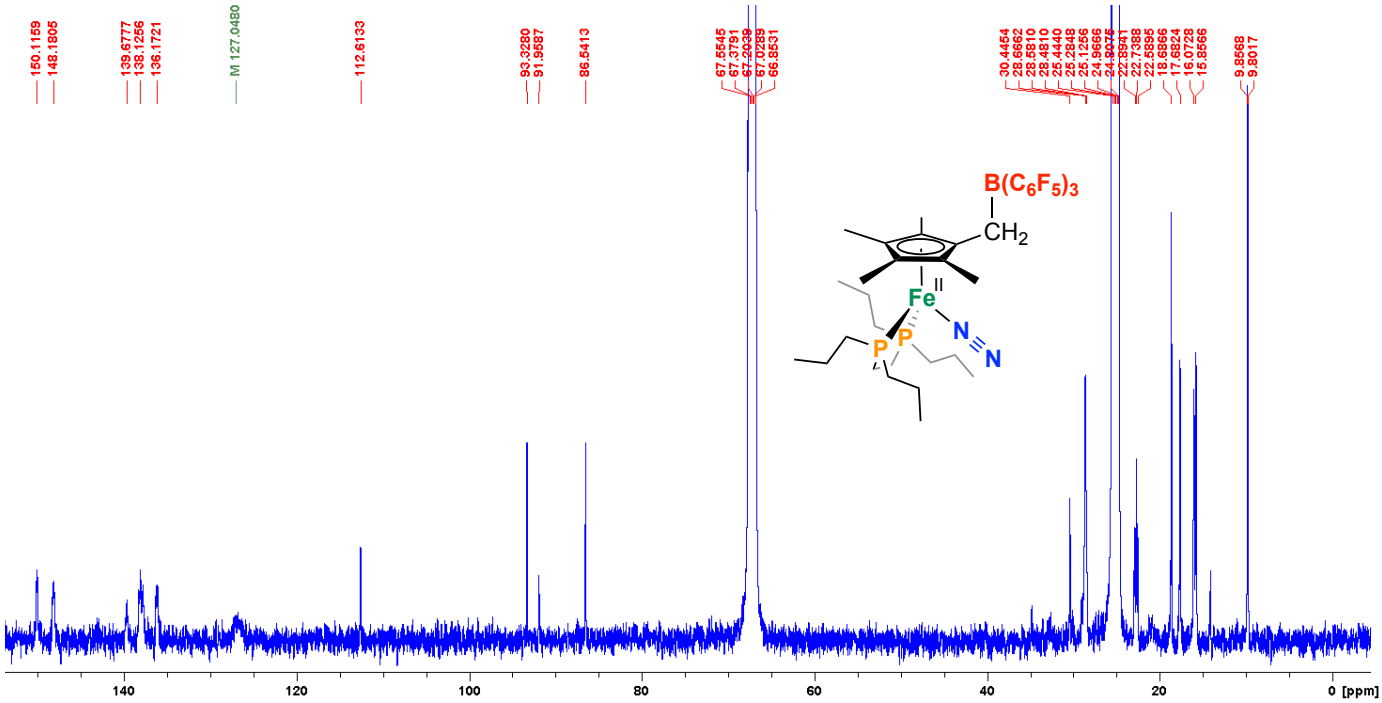

Figure S28: 6, FT-IR ATR, 298 K ($\nu[N_2]$ = 2093 cm^{-1}).

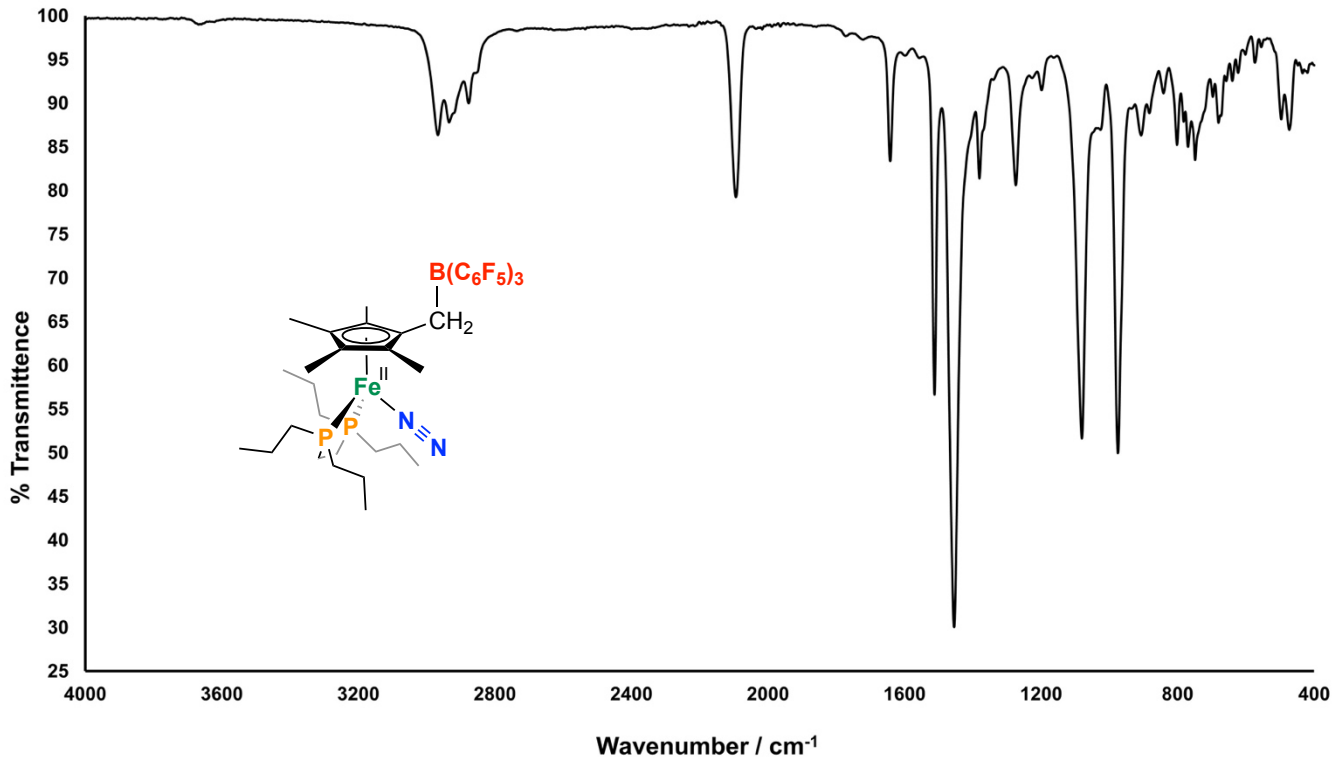

Figure S29: 7, ^{1}H NMR, C_6D_6, 500 MHz, 298 K. Note that the integral value for the [Fe]–H signal is lower than expected. This has been observed for other [Fe]-hydrides reported by our group[3,4] and can be attributed to relaxation time.

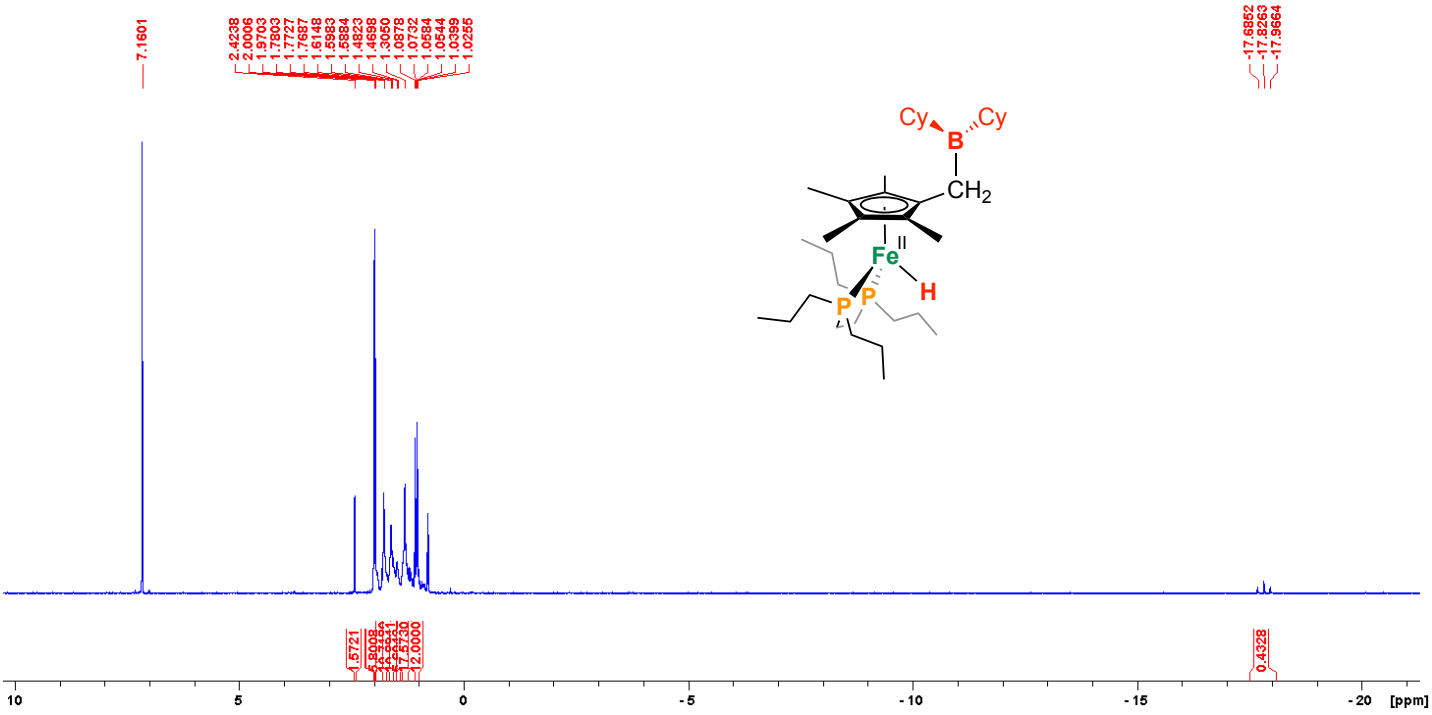

Figure S30: 7, ^{1}H NMR, C_6D_6, 500 MHz, 298 K – expansion of the alkyl region.
* = residual pentane solvent.

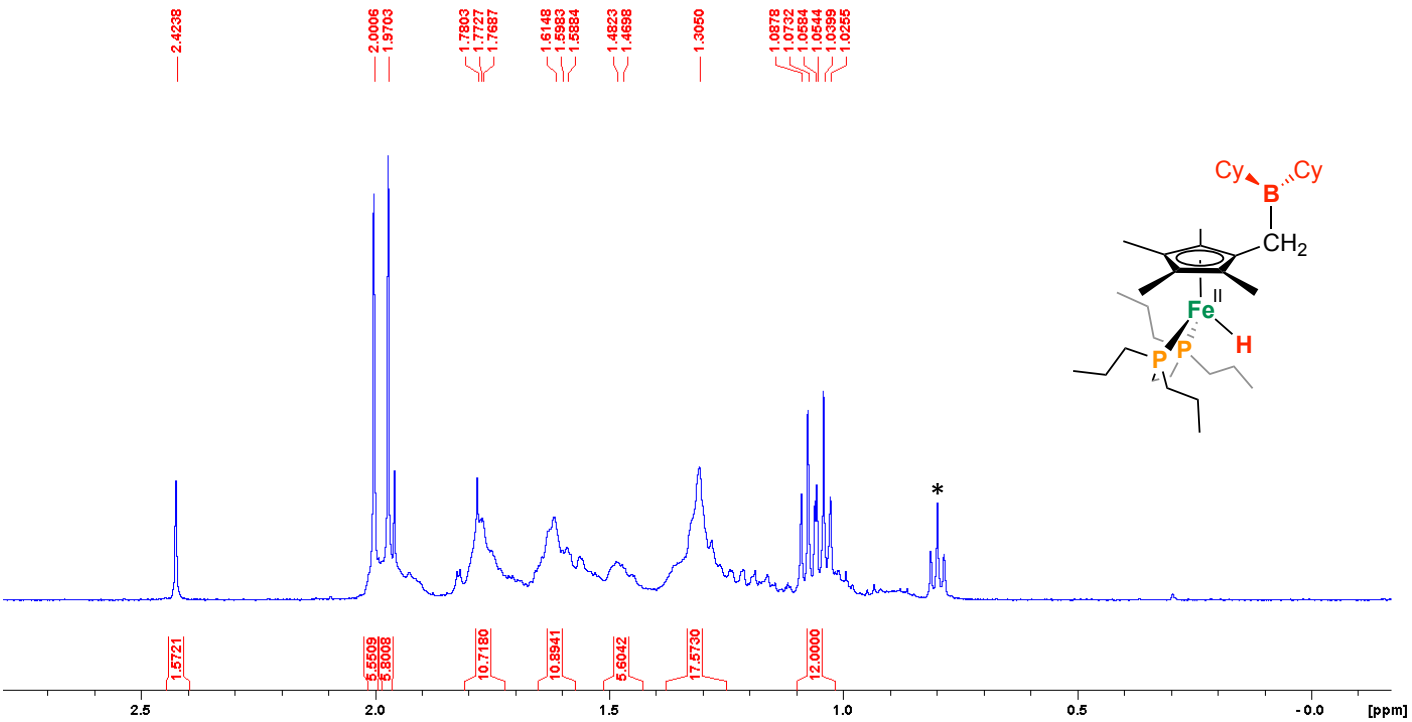

Figure S31: 7, ^{1}H NMR, C_6D_6, 500 MHz, 298 K – expansion of the [Fe]–H signal.

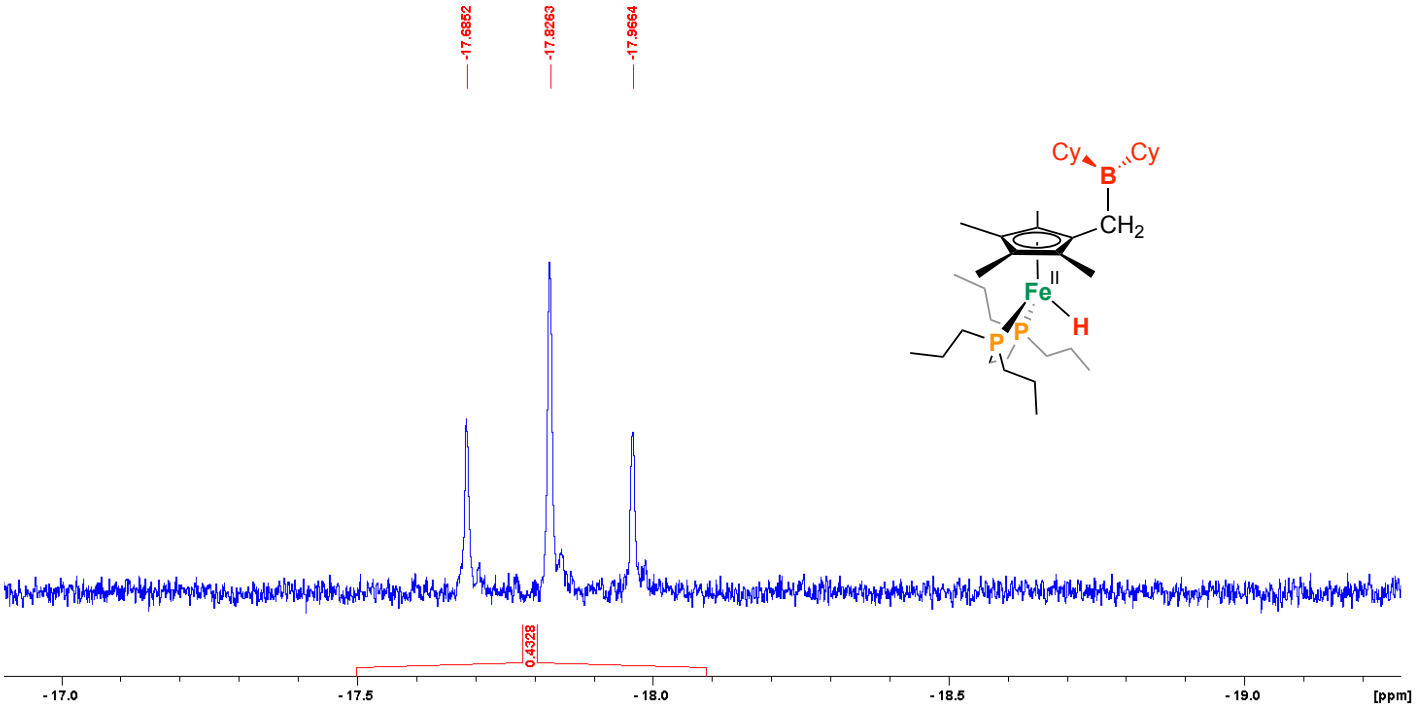

Figure S32: 7, $^{31}P\{^{1}H\}$ NMR, C_6D_6, 202.5 MHz, 298 K.

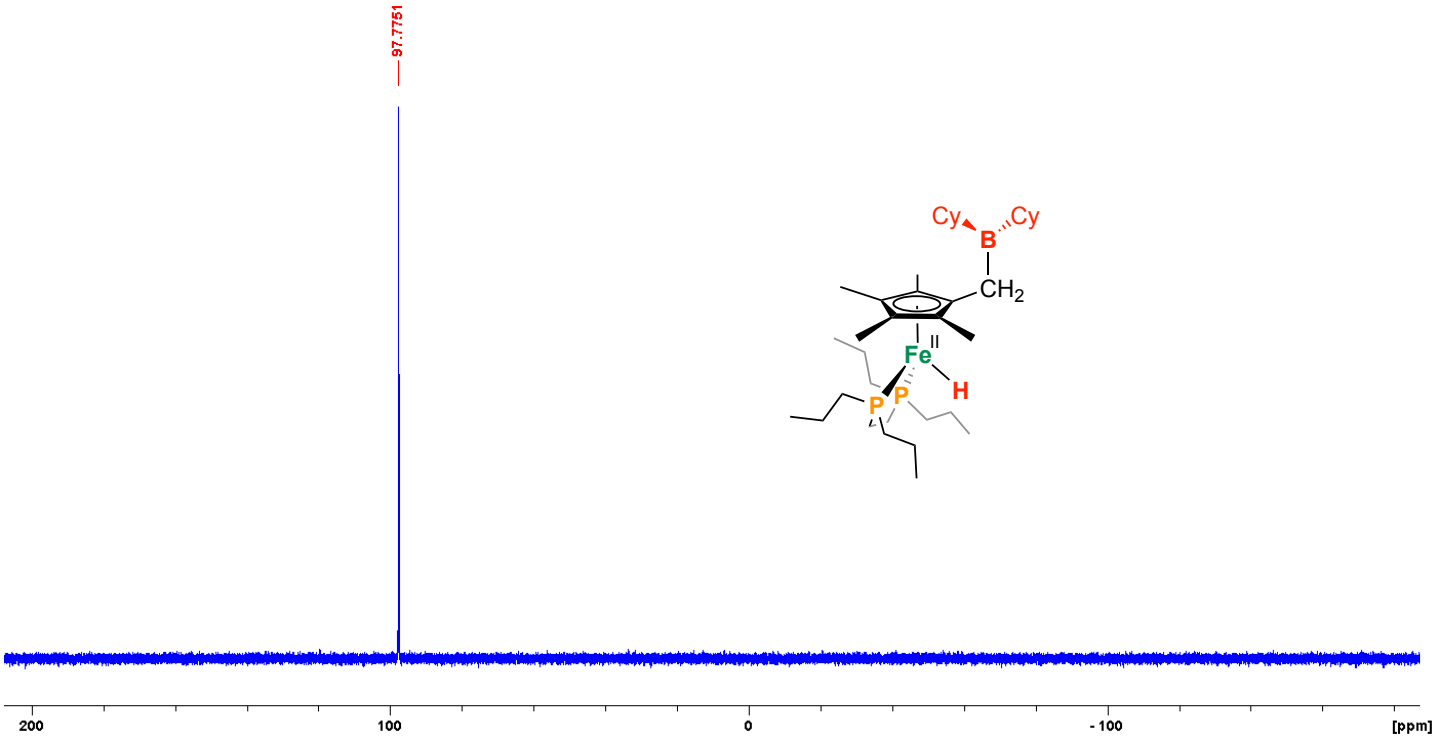

Figure S33: 7, $^{11}B\{^{1}H\}$ NMR, C_6D_6, 160.5 MHz, 298 K.

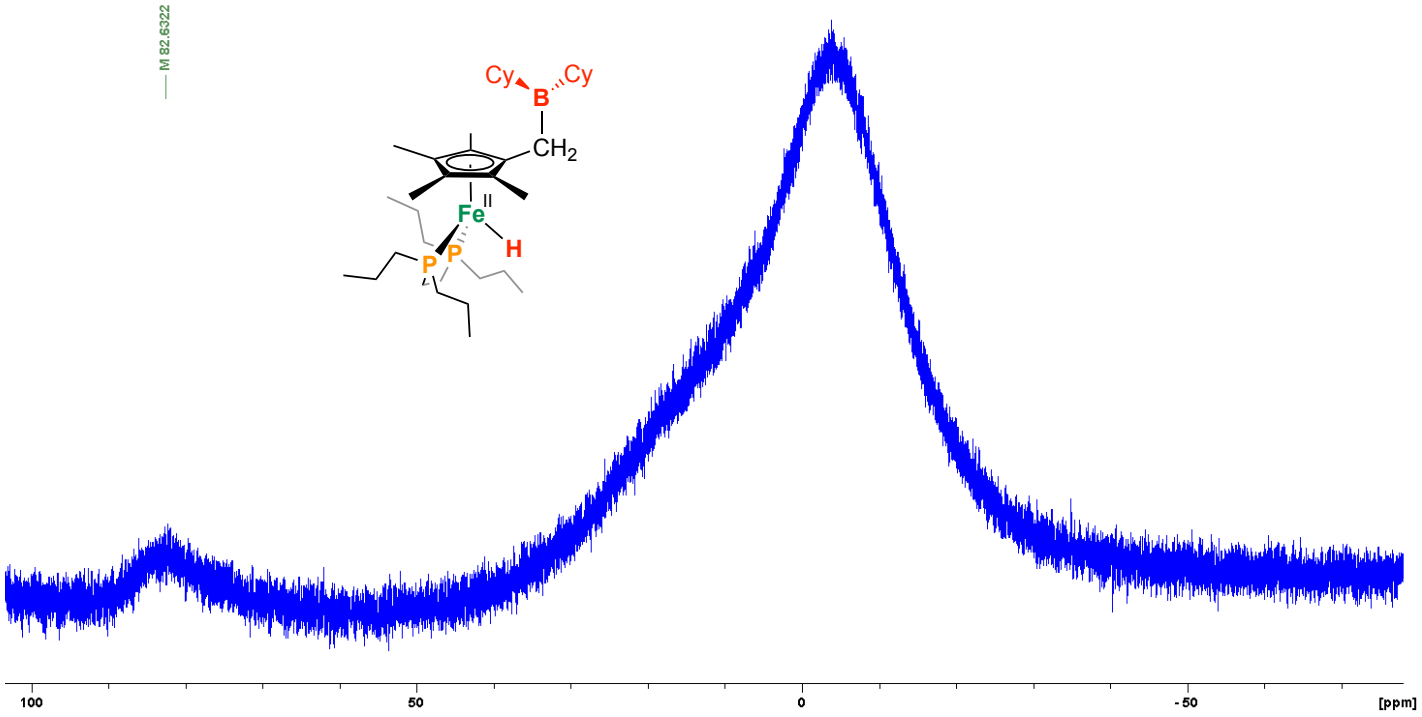

Figure S34: 7, $^{13}C\{^{1}H\}$ NMR, C_6D_6, 125.8 MHz, 298 K.

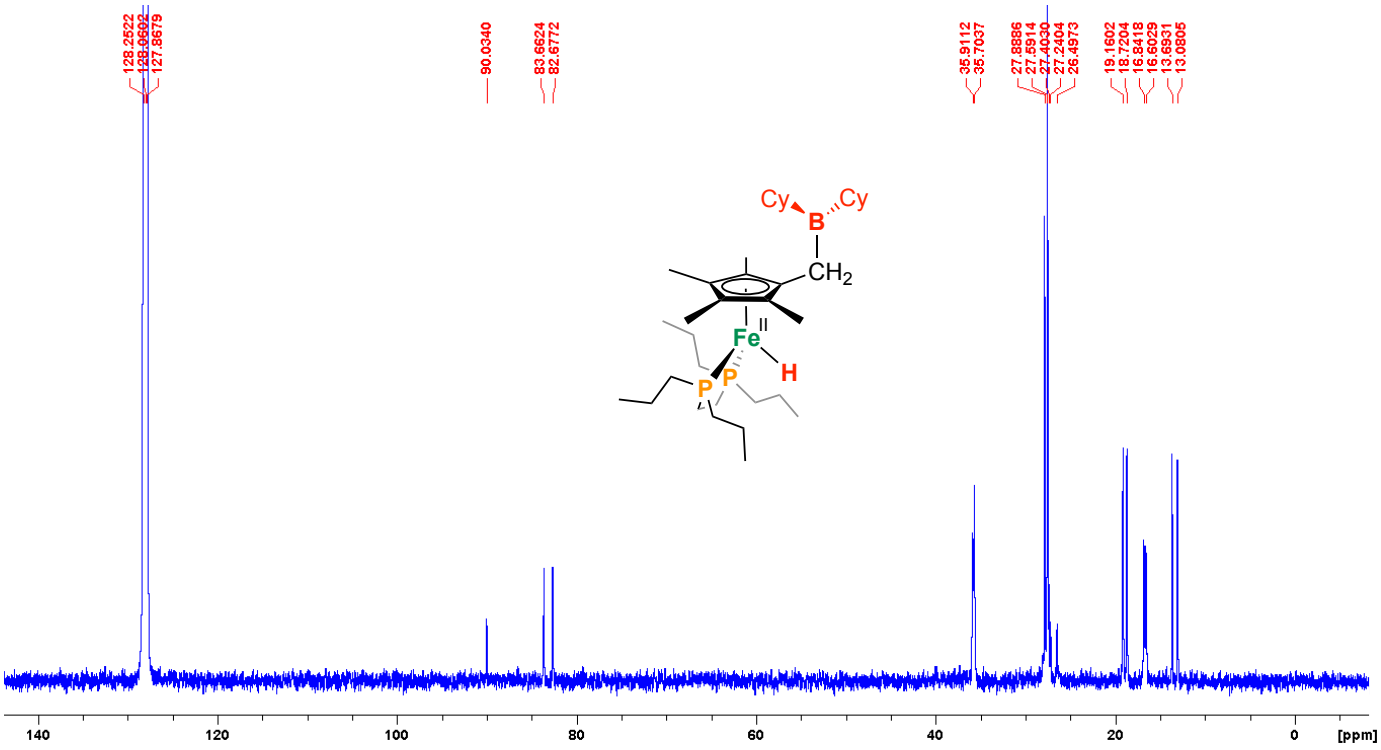

Figure S35: 7, FT-IR ATR, 298 K (ν[Fe–H] = 1844 cm^{-1}).

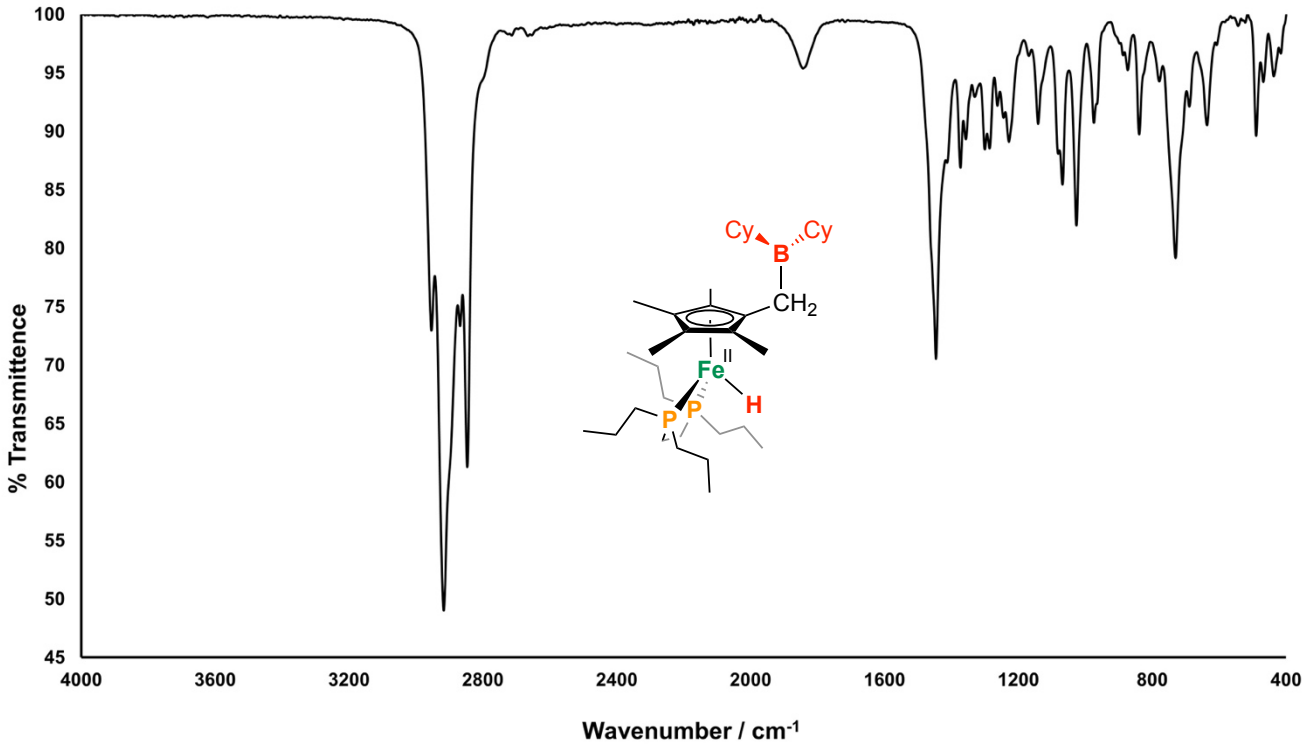

X-Ray Crystallography:

Single crystal X-Ray diffraction (scXRD) data for X was collected using a Bruker D8 Venture diffractometer equipped with an Apex detector having a Cu/Mo IμS microsource at the University of Windsor. All crystals were mounted on a MiTeGen loop.

Cell refinement and data reduction were performed using Apex3.[5] An empirical absorption correction based on multiple measurements of equivalent reflections and merging of data was performed using SADABS.[6] Data conversion from XDS to SADABS file format was performed using XDS2SAD.[7] The space group was confirmed by XPREP.[8]

Routine checkCIF and structure factor analyses were performed using Platon.[9] CCDC **2266746-2266749** contains the supplementary crystallographic data for this paper. These data can be obtained free of charge from The Cambridge Crystallographic Data Centre *via* www.ccdc.cam.ac.uk/data_request/cif.

Table S1. Crystallographic data for **1** and **2**.

Compound	**1**	**2**
Empirical formula	$C_{48}H_{67}BFeN_2P_2$	$C_{24}H_{46}FeP_2$
Formula weight	800.63	452.40
Temperature/K	170.0	170.0
Crystal system	Triclinic	Triclinic
Space group	*P-1*	*P-1*
a/Å	10.4118(10)	8.3558(12)
b/Å	14.7221(14)	9.4334(16)
c/Å	15.2322(16)	16.5656(18)
α/°	96.196(4)	82.946(9)
β/°	93.280(4)	82.104(9)
γ/°	105.849(4)	77.117(8)
V/Å^3	2223.8(4)	1255.1(3)
Z	2	2
ρ_{calc} g/cm^{-3}	1.196	1.197
μ/ mm^{-1}	0.445	0.735
F(000)	860.0	492.0
Crystal size/ mm^3	0.1 x 0.07 x 0.05	0.17 x 0.07 x 0.03
Radiation	MoK$_\alpha$ (λ =0.71073)	MoK$_\alpha$ (λ = 0.71073)
2θ range for data collection/°	5.92 to 52.94	4.45 to 56.652
Index ranges	-13 ≤ h ≤ 13, -18 ≤ k ≤ 18, -19 ≤ l ≤ 19	-11 ≤ h ≤ 11, -12 ≤ k ≤ 12, -22 ≤ l ≤ 22
Independent reflections	9147 [R_{int} = 0.0916, R_{sigma} = 0.0381]	6237 [R_{int} = 0.0547, R_{sigma} = 0.0227]
Data/restraints/parameters	9147/1352/659	6237/0/252
Goodness-of-fit on F^2	1.029	1.0064
R [I>=2θ (I)] (R1, wR2)	R_1 = 0.0542, wR_2 = 0.1317	R_1 = 0.0283, wR_2 = 0.0656
R (all data) (R1, wR2)	R_1 = 0.0753, wR_2 = 0.1458	R_1 = 0.0369, wR_2 = 0.0703
Largest diff. peak/hole / (e Å^{-3})	1.06/-0.96	0.32/-0.30

$R1 = \Sigma \, ||F_o|-|F_c|| \, / \, \Sigma \, |F_o|$; $wR2 = [\Sigma(w(F_o^2 - F_c^2)^2) / \Sigma \, w(F_o^2)^2]^{1/2}$

Table S2. Crystallographic data for **3** and (±)-**4**.

Compound	**3**	(±)-**4**
Empirical formula	$C_{25}H_{46}FeO_2P_2$	$C_{31}H_{52}FeOP_2$
Formula weight	496.41	558.51
Temperature/K	170.0	170.0
Crystal system	Monoclinic	Triclinic
Space group	*P2₁/c*	*P-1*
a/Å	18.7645(10)	9.790(14)
b/Å	8.6734(4)	10.43(2)
c/Å	16.7609(9)	16.32(2)
α/°	90	84.54(8)
β/°	100.195(2)	89.08(5)
γ/°	90	67.93(5)
V/Å^3	2684.8(2)	1537(4)
Z	4	2
ρ_{calc} g/cm^{-3}	1.228	**
μ/ mm^{-1}	0.699	**
F(000)	1072.0	**
Crystal size/ mm^3	0.15 x 0.04 x 0.02	**
Radiation	MoK_α (λ =0.71073)	**
2θ range for data collection/°	4.938 to 56.682	**
Index ranges	-25 ≤ h ≤ 25, -11 ≤ k ≤ 11, -22 ≤ l ≤ 22	**
Independent reflections	6700 [R_{int} = 0.0543, R_{sigma} = 0.0263]	**
Data/restraints/parameters	6700/0/279	**
Goodness-of-fit on F^2	1.063	**
R [I>=2θ (I)] (R1, wR2)	R_1 = 0.0278, wR_2 = 0.0682	**
R (all data) (R1, wR2)	R_1 = 0.0320, wR_2 = 0.0714	**
Largest diff. peak/hole / (e Å^{-3})	0.49/-0.22	**

** = Connectivity map only

$R1 = \Sigma \, ||F_o|-|F_c|| \, / \, \Sigma \, |F_o|$; $wR2 = [\Sigma(w(F_o^2 - F_c^2)^2) / \Sigma \, w(F_o^2)^2]^{1/2}$

Figure S36. Connectivity map of (±)-**4**. Protons omitted for clarity except on η⁵-C_5Me_4–$C\underline{H}_2$–PhC$\underline{H}$O.

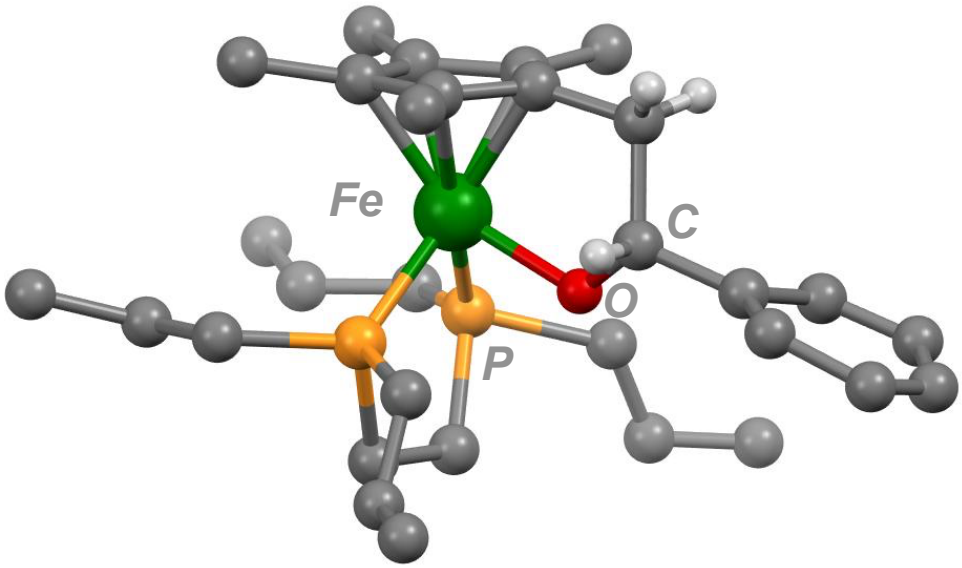

Table S3. Crystallographic data for **6**.

Compound	**6**
Empirical formula	$C_{42}H_{46}BF_{15}FeN_2P_2$
Formula weight	992.41
Temperature/K	170.0
Crystal system	Orthorhombic
Space group	*Pca21*
a/Å	24.1488(9)
b/Å	9.1691(4)
c/Å	20.0496(6)
α/°	90
β/°	90
γ/°	90
V/Å^3	4439.4(3)
Z	4
ρ_{calc} g/cm^{-3}	1.485
μ/ mm^{-1}	0.508
F(000)	2032.0
Crystal size/ mm^3	0.15 x 0.1 x 0.02
Radiation	MoK$_\alpha$ (λ =0.71073)
2θ range for data collection/°	3.989 to 56.728
Index ranges	-32 ≤ h ≤ 32, -12 ≤ k ≤ 12, -26 ≤ l ≤ 26
Independent reflections	11077 [R_{int} = 0.0744, R_{sigma} = 0.0227]
Data/restraints/parameters	11077/6/575
Goodness-of-fit on F^2	1.057
R [I>=2θ (I)] (R1, wR2)	R_1 = 0.0330, wR_2 = 0.0759
R (all data) (R1, wR2)	R_1 = 0.0434, wR_2 = 0.0831
Largest diff. peak/hole / (e Å^{-3})	0.48/-0.40

$R1 = \Sigma \, ||F_o|-|F_c|| \, / \, \Sigma \, |F_o|$; $wR2 = [\Sigma(w(F_o^2 - F_c^2)^2) / \Sigma \, w(F_o^2)^2]^{1/2}$

Computational Details:

All calculations were performed using version 5.0.3 of the ORCA computational package[10] and were run on the Graham cluster maintained by Compute Canada. All geometry optimizations and frequency calculations were performed at the BP86-D3(BJ)/def2-TZVP level of theory.[11] The RI approximation was used to enhance computational efficiency, along with the auxiliary basis *def2/J*. [12] Convergence criteria were met using the *defgrid2* integral grid size. Frequency calculations (*Freq*) were performed to confirm that each optimized geometry was a true minimum indicated by the absence of imaginary frequencies. Single-point calculations were performed at the BP86-D3(BJ)/def2-TZVP level of theory on optimized geometries.

Accurate electronic energies were determined using CCSD(T) at the DLPNO-CCSD(T)/def2-TZVP level of theory. [13] The RIJCOSX approximation was used to enhance computational efficiency, along with a *def2/J* auxiliary basis set.[14] As well, a *def2-TZVP/C* auxiliary basis set was used.[15]

To obtain accurate thermochemical information, the final Gibbs free energies for each chemical species were calculated using the following equation.

$$\Delta G_{solv} = E_{el}(DLPNO\text{-}CCSD(T)) + \Delta G_{correction}(DFT) + \Delta G^{\circ}_{solv}(DFT).$$

$E_{el}(DLPNO\text{-}CCSD(T))$ is the final electronic energy from a DLPNO-CCSD(T)/def2-TZVP calculation, $\Delta G_{correction}(DFT)$ is the $G\text{-}E_{el}$ (Gibbs free energy minus the electronic energy) from a BP86-D3(BJ)/def2-TZVP calculation, and $\Delta G^{\circ}_{solv}(DFT)$ is the sum of $\Delta G_{ENP}(CPCM\ Dielectric)$ and $\Delta G_{CDS}(Free\text{-}energy(cav+disp))$ from an *SMD* single point calculation.

Wiberg bond indices (WBIs) were calculated at the BP86-D3(BJ)/def2-TZVPP level of theory using the Multiwfn program.[16]

NBOs were calculated using the NBO 7.0[17] program implemented with Gaussian 16, revision C.01.[18] The D3(BJ) dispersion correction was used along with the BP86 functional and the def2-TZVPP basis set. NBOs were visualized in Avogadro.[19]

Figure S37. NBOs showcasing the bonding between Fe1 and the two carbon atoms of the exocyclic alkenyl fragment on the fulvene ligand of **2**. Atomic contributions are in parentheses.

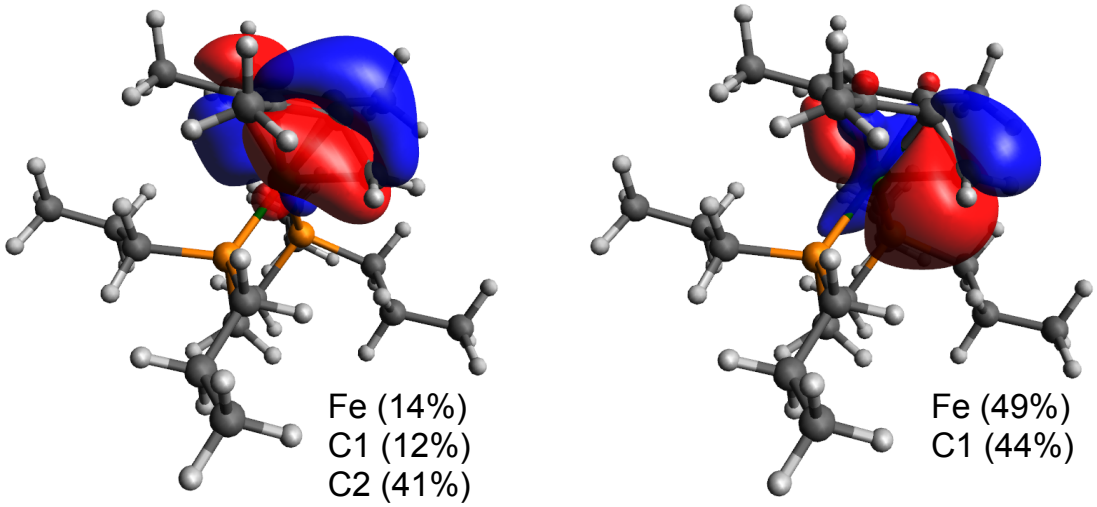

Table S4. Wiberg bond index (WBI) data from DFT calculations on **2**.

Atom pair	Wiberg bond index (WBI)
C1-C2	1.33
C2-C3	1.11
C3-C4	1.21
C4-C5	1.21
C5-C6	1.21
C6-C2	1.11
Fe1-C1	0.70
Fe1-C2	0.70
Fe1-C3	0.60
Fe1-C4	0.52
Fe1-C5	0.52
Fe1-C6	0.60

Figure S38. Computationally-determined thermodynamics for deprotonation of either a methyl group on a Cp*-ring or d*n*ppe propyl arm. Energy calculated using DLPNO-CCSD(T).

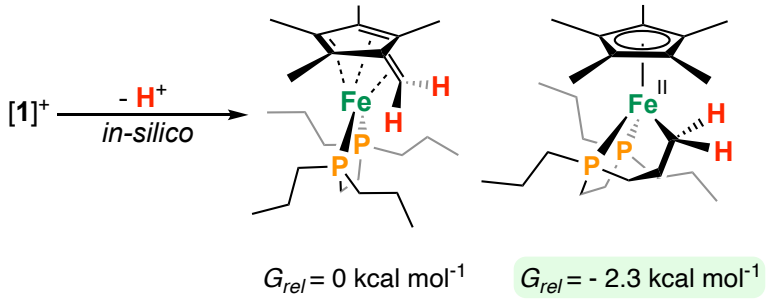

The thermodynamics of generating the tucked-in complex **2** were examined. Specifically, we were interested to see if it was more favourable to deprotonate one of the methyl groups on the d*n*ppe ligand (to generate a stable five-membered ferra(II)cycle) or deprotonate the Cp*(C<u>H</u>$_3$) ligand. This investigation was prompted by a previous study, where we observed such five-membered ferra(II)cyclized products, speaking to their ease of access.[3] Starting with [**1**]$^+$, we found that deprotonation of the d*n*ppe(C<u>H</u>$_3$) arm was favoured by 2.3 kcal mol^{-1}, indicating that formation of **2** is likely a kinetic effect.

References:

[1] Drover, M.W.; Dufour, M.C.; Lesperance-Nantau, L.A.; Noriega, R.P.; Levin, K.; Schurko, R.W. *Chem. Eur. J.* **2020**, *26*, 11180-11186.
[2] Abiko, A. *Org. Synth.* **2003**, *79*, 103.
[3] Zurakowski, J.A.; Brown, K.R.; Drover, M.W. *Inorg. Chem.* **2023**, *62*, 7053-7060.
[4] a) Zurakowski, J.A.; Bhattacharyya, M.; Spasyuk, D.M.; Drover, M.W. *Inorg. Chem.* **2021**, *60*, 37.
[5] Bruker (2016). APEX3, SAINT, and SADBAS. Bruker AXS Inc., Madison, Wisconsin, USA.
[6] Krause, L; Herbst-Irmer, R.; Sheldrick, G.M.; Stalke, S. *J. Appl. Cryst.* **2015**, *48*, 3.
[7] XDS2SAD, Sheldrick, G.M. **2008**, University of Gottingen, Germany.
[8] a) XPREP, **2014**, Bruker AXS Inc., Madison, Wisconsin, USA.; b) XPREP Version **2008**, Sheldrick, G.M. **2008**, Bruker AXS Inc., Madison, Wisconsin, USA.
[9] Spek, A.L. Structure validation in chemical crystallography. *Acta Cryst*. **2009**, *D65*, 148.
[10] Neese, F. Software Update: The ORCA Program – Version 5.0. *WIREs Comput. Mol. Sci.*, **2022**, *12*, e1606.
[11] a) S. Grimme, S. Ehrlich, L. Goerigk, *J. Comput. Chem.* **2011**, *32*, 1456; b) S. Grimme, J. Antony, S. Ehrlich, H. Krieg, *J. Chem. Phys.* **2010**, *132*, 154104; c) F. Weigend, R. Ahlrichs, *Phys. Chem. Chem. Phys.* 2005, **7**, 3297.
[12] F. Weigend, *Phys. Chem. Chem. Phys*. **2006**, *8*, 1057.
[13] a) C. Riplinger, P. Pinski, U. Becker, E.F. Valeeve, F. Neese, *J. Chem. Phys.* **2016**, *144*, 024109; b) C. Riplinger, B. Sandhoefer, A. Hansen, F. Neese, *J. Chem. Phys*. **2013**, *139*, 134101; c) C. Riplinger, F. Neese, *J. Chem. Phys.* **2013**, *138*, 034106.
[14] A. Hellweg, C. Hattig, S. Hofener, W. Klopper, *Theor. Chim. Acta* **1990**, *77*, 123.
[15] a) G. Knizia, J.E.M.N. Klein, *Angew. Chem. Int. Ed.* **2015**, *54*, 5518; b) G. Knizia, *J. Chem. Theory Comput.* **2013**, *9*, 4834.
[16] Tian Lu, Feiwu Chen, Multiwfn: A Multifunctional Wavefunction Analyzer, *J. Comput. Chem.* **33**, 580-592 (2012) DOI: 10.1002/jcc.22885
[17] NBO 7.0. E. D. Glendening, J, K. Badenhoop, A. E. Reed, J. E. Carpenter, J. A. Bohmann, C. M. Morales, P. Karafiloglou, C. R. Landis, and F. Weinhold, Theoretical Chemistry Institute, University of Wisconsin, Madison (2018).
[18] Gaussian 16, Revision C.01, M. J. Frisch, G. W. Trucks, H. B. Schlegel, G. E. Scuseria, M. A. Robb, J. R. Cheeseman, G. Scalmani, V. Barone, G. A. Petersson, H. Nakatsuji, X. Li, M. Caricato, A. V. Marenich, J. Bloino, B. G. Janesko, R. Gomperts, B. Mennucci, H. P. Hratchian, J. V. Ortiz, A. F. Izmaylov, J. L. Sonnenberg, D. Williams-Young, F. Ding, F. Lipparini, F. Egidi, J. Goings, B. Peng, A. Petrone, T. Henderson, D. Ranasinghe, V. G. Zakrzewski, J. Gao, N. Rega, G. Zheng, W. Liang, M. Hada, M. Ehara, K. Toyota, R. Fukuda, J. Hasegawa, M. Ishida, T. Nakajima, Y. Honda, O. Kitao, H. Nakai, T. Vreven, K. Throssell, J. A. Montgomery, Jr., J. E. Peralta, F. Ogliaro, M. J. Bearpark, J. J. Heyd, E. N. Brothers, K. N. Kudin, V. N. Staroverov, T. A. Keith, R. Kobayashi, J. Normand, K. Raghavachari, A. P. Rendell, J. C. Burant, S. S. Iyengar, J. Tomasi, M. Cossi, J. M. Millam, M. Klene, C. Adamo, R. Cammi, J. W. Ochterski, R. L. Martin, K. Morokuma, O. Farkas, J. B. Foresman, and D. J. Fox, Gaussian, Inc., Wallingford CT, 2019.

[19] a) Avogadro: an open-source molecular builder and visualization tool. Version 1.20. http://avogadro.cc/ b) Marcus D. Hanwell, Donald E. Curtis, David C. Lonie, Tim Vandermeersch, Eva Zurek and Geoffrey R. Hutchison; "Avogadro: An advanced semantic chemical editor, visualization, and analysis platform" *Journal of Cheminformatics* **2012**, 4:17.